Chapter 1—
Introduction

1.1—
Introduction

The twin subjects of fractal geometry and chaotic dynamics have been behind an enormous change in the way scientists and engineers perceive, and subsequently model, the world in which we live. Chemists, biologists, physicists, physiologists, geologists, economists, and engineers (mechanical, electrical, chemical, civil, aeronautical etc) have all used methods developed in both fractal geometry and chaotic dynamics to explain a multitude of diverse physical phenomena: from trees to turbulence, cities to cracks, music to moon craters, measles epidemics, and much more. Many of the ideas within fractal geometry and chaotic dynamics have been in existence for a long time, however, it took the arrival of the computer, with its capacity to accurately and quickly carry out large repetitive calculations, to provide the tool necessary for the in-depth exploration of these subject areas. In recent years, the explosion of interest in fractals and chaos has essentially ridden on the back of advances in computer development.

The objective of this book is to provide an elementary introduction to both fractal geometry and chaotic dynamics. The book is split into approximately two halves: the first—chapters 2–4—deals with fractal geometry and its applications, while the second—chapters 5–7—deals with chaotic dynamics. Many of the methods developed in the first half of the book, where we cover fractal geometry, will be used in the characterization (and comprehension) of the chaotic dynamical systems encountered in the second half of the book. In the rest of this chapter brief introductions to fractal geometry and chaotic dynamics are given, providing an insight to the topics covered in subsequent chapters of the book.

1.2—
A Matter of Fractals

In recent years, the science of fractal geometry has grown into a vast area of knowledge, with almost all branches of science and engineering gaining from the new insights it has provided. Fractal geometry is concerned with the properties of fractal objects, usually simply known as **fractals.** Fractals may be found in nature or generated using a mathematical recipe. The word 'fractal' was coined by Benoit Mandelbrot, sometimes referred to as the father of fractal geometry. Mandelbrot realized that it is very often

impossible to describe nature using only Euclidean geometry, that is in terms of straight lines, circles, cubes, and such like. He proposed that fractals and fractal geometry could be used to describe real objects, such as trees, lightning, river meanders and coastlines, to name but a few.

There are many definitions of a fractal. Possibly the simplest way to define a fractal is as an object *which appears self-similar under varying degrees of magnification. In effect, possessing symmetry across scale, with each small part of the object replicating the structure of the whole.* This is perhaps the loosest of definitions, however, it captures the essential, defining characteristic, that of **self-similarity.** A diagram is possibly the best way to illustrate what is meant by a fractal object. Figure 1.1 contains sketches of two naturally occurring 'objects': an island coastline and a person. As we zoom into the coastline, we find that its ruggedness is repeated on finer and finer scales, and under rescaling looks essentially the same: the coastline is a fractal curve. The person, however, is not a self-similar object. As we zoom into various parts of the body, we see quite different forms. The hand does not resemble the whole body, the fingernail does not look like the hand and so on. Even viewing different parts of the body at the same scale, say the hand and the head, we would see that again they are not similar in form. We conclude that a person is not a fractal object. It is interesting to note at this stage that, although the body as a whole is not a fractal object, recent studies have attempted, with some success, to characterize certain parts of the body using fractal geometry, for example, the branching structure of the lung and the fine structure of the neuron (brain cell).
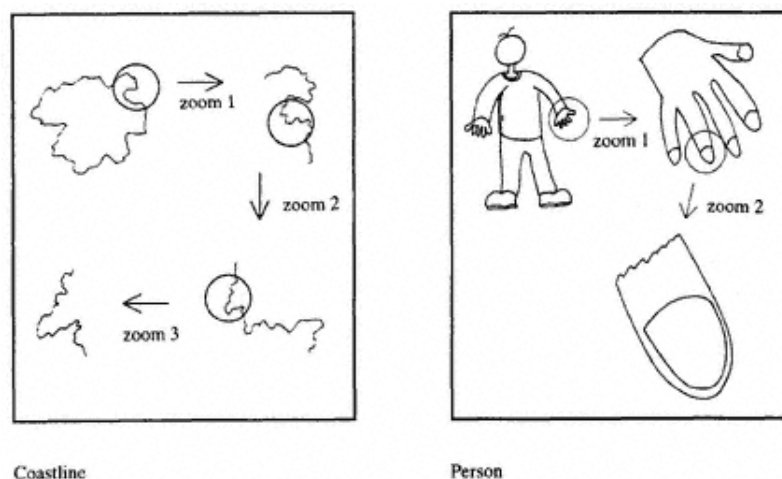

Figure 1.1.
Fractal and non-fractal objects.

Figure 1.2 contains four **natural fractals:** the boundary of clouds, wall cracks, a hillside silhouette and a fern. All four possess self-similarity. The first three natural fractals possess the same statistical properties (i.e. the same degree of ruggedness) as we zoom in. They possess **statistical self-similarity.** On the other hand, the fern possesses

Cloud outlines

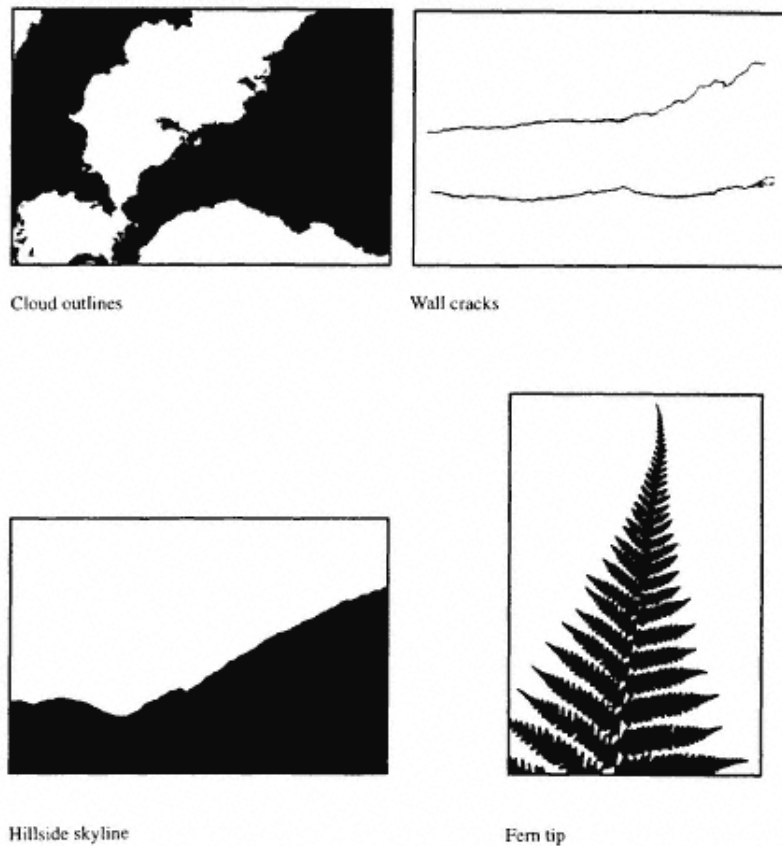Wall cracks

Hillside skyline

Fern tip

Figure 1.2.
Natural fractal objects.

exact self-similarity. Each frond of the fern is a mini-copy of the whole fern, and each frond branch is similar to the whole frond, and so on. In addition, as we move towards the top of the fern we see a smaller and smaller copy of the whole fern. The fractals of figure 1.2 require a two-dimensional (2D) plane to 'live in', that is all the points on them can be specified using only two co-ordinates. Put more formally, they have a Euclidean dimension of two. However, many natural fractals need a 3D world in which to exist. Take, for example, a tree whose branches weave through three dimensions; see the tree branching in 3D in figure 1.3 (if you can!). Fractals themselves have their own dimension, known as the **fractal dimension,** which is usually (but not always) a noninteger dimension that is greater than their topological dimension, D_T, and less than their Euclidean dimension D_E (see chapter 2). There are many definitions of fractal dimension and we shall encounter a number of them as we proceed through the text, including: the similarity dimension, D_S; the divider dimension, D_D; the Hausdorff dimension, D_H; the box counting dimension, D_B; the correlation dimension, D_C; the information

dimension, D_I; the pointwise dimension D_P; the averaged pointwise dimension, D_A; and the Lyapunov dimension D_L. The last seven dimensions listed are particularly useful in characterizing the fractal structure of strange attractors associated with chaotic dynamics.
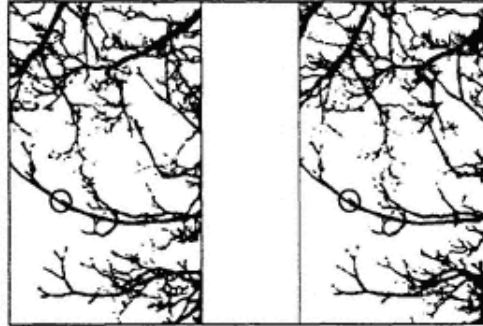

Figure 1.3.
Tree branching in 3D. To see the 3D image, illuminate
the page with a good even source of light: daylight is by
far the best. Keeping the page still, view the images
from a distance of 15–20 cm, let your eyes relax and
try to merge the two circles. After merging, the image
should come into focus within a few seconds. Once
focused, let your eyes wander around the image
to see 3D. The technique needs a little practice:
the trick is to focus on the merged image without
the two constituent images diverging, but
persistence usually pays off.

We make one more important distinction between fractals which are self-similar everywhere and those which are self-similar only if we look in the right place. Examples are given in figure 1.4. The figure contains three **mathematical fractals,** these are: a logarithmic spiral, a binary tree, and a Sierpinski gasket. We see self-similarity in the logarithmic spiral of figure 1.4(*a*) only if we zoom into its point of convergence. The part of the spiral contained within box A contains the point of convergence, hence infinitely many scaled copies of the spiral exist within this area. However, the part of the spiral within box B does not contain the point of convergence and hence does not contain scaled down replicas of the whole log spiral. The binary tree (figure 1.4(*b*)) is simple to construct mathematically: we simply add further, scaled down, T-shaped branches to the ends of the previous branches. After an infinite number of branch additions we have the binary tree. As we zoom into the branches of the binary tree we see more and more detail, consisting of exactly self-similar copies of the whole tree. Hence, it is a fractal. However, the self-similarity of the binary tree (figure 1.4(*b*)) is only evident if we zoom into one of its branch ends. The circled area A contains one such branch end, which is an exact copy of the whole tree scaled down by one eighth. Contrast this with the part of the tree contained within the circled area B which is not a scaled down copy of the whole tree. The Sierpinski gasket of figure 1.4(*c*) (the construction of which is detailed in chapter 2) is self-similar everywhere. No matter where we zoom into the gasket, we will see further copies of the whole gasket. This property is known as **strict self-similarity** and the Sierpinski gasket is a strictly self-similar fractal. In this book we will concentrate on strictly self-similar fractals. In figure 1.2 the cloud boundary, wall
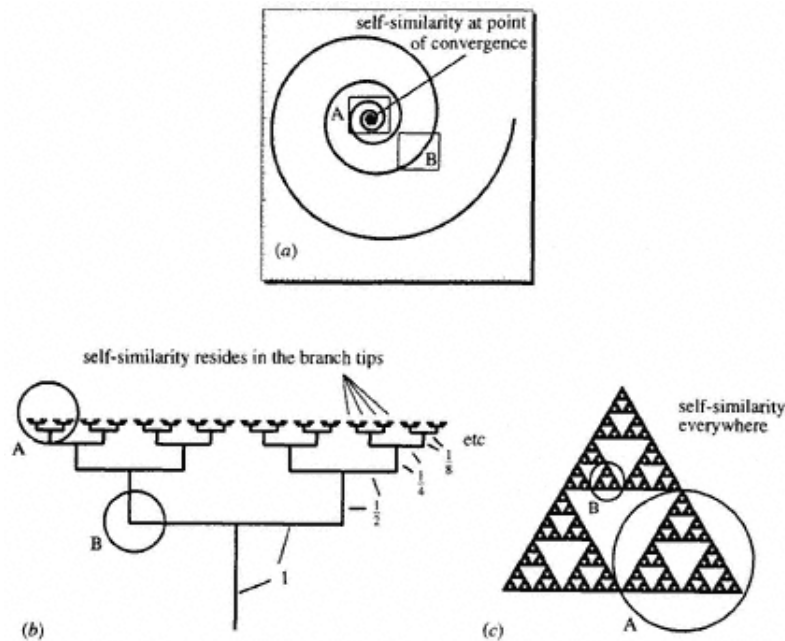
Figure 1.4.
The nature of self-similarity. (*a*) The log spiral is self-similar only at
its point of convergence. (*b*) The binary tree is self-similar only at
the branch tips. (*c*) The Sierpinski gasket is self-similar everywhere.

crack, and hillside skyline are strictly self-similar, whereas the fern of figure 1.2 and the tree of figure 1.3 are only self-similar at their branch ends.

One last point worth noting is that even the best examples of natural fractals do not possess self-similarity at all scales, but rather over a sufficiently large range to allow fractal geometric methods to be successfully employed in their description. On the other hand, mathematical fractals can be specified to infinite precision and are thus self-similar at all scales. The distinction between the two is usually blurred in the literature, however, it is one worth remembering if you intend using, in a practical situation, some of the methods from fractal geometry learned from this text.

1.3—
Deterministic Chaos.

Oscillations are to be found everywhere in science and nature. The mechanical engineer may be concerned with the regular oscillation of an out of balance drive shaft; the civil engineer with the potentially disastrous structural vibrations induced by vortex shedding on a bridge deck; the electrical engineer with the oscillatory output from nonlinear circuits; the chemist/chemical engineer with the regular cycling of a chemical reaction; the geologist/geophysicist with earthquake tremors; the biologist with the cycles of growth and decay in animal populations; the cardiovascular surgeon with the regular

(and more so, irregular) beating of the human heart; the economist with the boom—bust cycles of the stock market; the physicist with the oscillatory motion of a driven pendulum; the astronomer with the cyclical motion of celestial bodies; and so on. (The list is extensive and diverse!)

Dynamical oscillators may be classified into two main categories: linear and nonlinear. In general, all real systems are nonlinear, however, very often it is the case that, as a first approximation to the dynamics of a particular system, a linear model may be used. Linear models are preferable from a scientist's point of view as typically they are much more amenable to mathematical analysis. (Hence the disproportionate number of linear systems studied in science.) Nonlinear systems, in contrast, are much more difficult to analyse mathematically, and, apart from a few exceptions, analytical solutions are not possible for the nonlinear differential equations used to describe their temporal evolution. In addition, only nonlinear systems are capable of a most fascinating behaviour known as **chaotic motion,** or simply **chaos,** whereby even simple nonlinear systems can, under certain operating conditions, behave in a seemingly unpredictable manner.
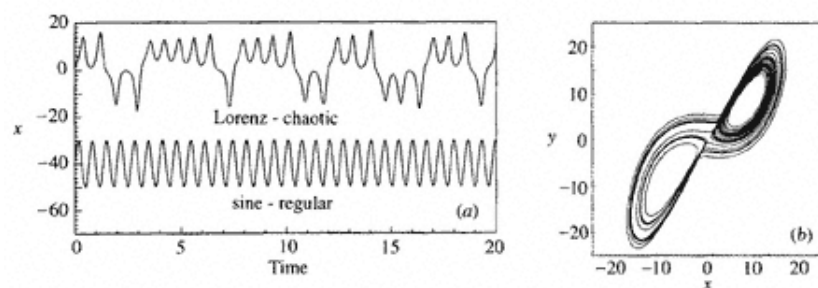

Figure 1.5.
Chaos and regularity. (*a*) Time series of the chaotic Lorenz model and a periodic
sinusoidal waveform. (*b*) Phase portrait of the Lorenz strange attractor.

In 1963 Edward Lorenz published his work entitled 'Deterministic nonperiodic flow' which detailed the behaviour of a simplified mathematical model representing the workings of the atmosphere. Lorenz showed how a relatively simple, **deterministic** mathematical model (that is, one with no randomness associated with it) could produce apparently unpredictable behaviour, later named chaos. The Lorenz model (see chapter 6) contains three variables: x, y and z. Figure 1.5(*a*) shows a chaotic time series output of the x variable of the Lorenz model. Notice that there is a recognizable structure to the time series: first the system oscillates in the positive-x region for a couple of oscillations, then it switches over to the negative x-region for a couple of oscillations, then back to the positive x-region for a few oscillations, and so on. However, the system never exactly repeats its behaviour. It would not matter how long we let the Lorenz model run for, we would never come across a repetition in the waveform. It is this aperiodic behaviour that is known as chaos. Compare it to the regular, periodic oscillations of the sinusoidal waveform (plotted below the Lorenz output) which repeats itself exactly and indefinitely. By plotting the Lorenz variables against each other, rather than against time, we can produce compact pictures of the system's dynamics. In two dimensions these are

known as phase portraits. The phase portrait for the Lorenz time series is shown in figure 1.5(*b*). Starting the Lorenz system from many initial conditions produces phase portraits all of the same form: the system is attracted towards this type of final solution. Figure 1.5(*b*) is then a plot of the long term behaviour of the Lorenz system and is known as the attractor of the system. If we zoom into the fine scale structure of the attractor for the chaotic Lorenz system we see that it has a fractal structure. The attractors for chaotic systems which have a fractal structure are termed **strange attractors.** The fractal structure of strange attractors may be examined using one or more of the definitions of fractal dimension mentioned in the above section. (See chapter 7 for more details.)

Chaos has now been found in all manner of dynamical systems; both mathematical models and, perhaps more importantly, natural systems. Chaotic motion has been observed in all of the 'real' oscillatory systems cited at the beginning of this section. In addition, many common qualitative and quantitative features can be discerned in the chaotic motion of these systems. This ubiquitous nature of chaos is often referred to as the **universality** of chaos.

1.4—
Chapter Summary and Further Reading

1.4.1—
Chapter Keywords and Key Phrases

fractals	*self-similarity*	*natural fractals*
statistical self-similarity	*exact self-similarity*	*fractal dimension*
mathematical fractals	*strict self-similarity*	*chaotic motion/chaos*
deterministic models	*strange attractors*	*universality*

1.4.2—
Further Reading

Non-mathematical treatments of the history and role of fractals and chaos in science, engineering and mathematics can be found in the books by Gleick (1987), Stewart (1989), Briggs and Peat (1989), Lorenz (1993) and Ruelle (1993). Also worth consulting is the highly readable collection of non-mathematical papers by leading experts from various fields edited by Hall (1992). The explosion in the number of scientific articles relating to chaos and fractals is shown graphically by Pickover (1992). Simple computer programs to generate a range of fractal and chaotic phenomena are given in the text by Bessant (1993). Other forms of medium worth consulting are the videos by Barlow and Gowan (1988) and Peitgen *et al* (1990), and also the freeware software package FRACTINT, widely available on the internet, user friendly, and of excellent quality. In fact, a search on the world wide web using the keywords 'fractal' or 'chaos' should yield a large amount of material, much of which is at a reasonably elementary level.

Chapter 2—
Regular Fractals and Self-Similarity

2.1—
Introduction

In this chapter we will examine some common mathematical fractals with structures comprising of <u>exact</u> copies of themselves at <u>all</u> magnifications. These objects possess **exact self-similarity** and are known as **regular fractals.** In chapter 1, a fractal object was loosely defined as one which appears self-similar at various scales of magnification and also as an object with its own **fractal dimension,** which is usually (but not always) a non-integer dimension greater than its topological dimension, D_T, and less than its Euclidean dimension, D_E. To date, there exists no watertight definition of a fractal object. Mandelbrot offered the following definition: 'A fractal is by definition a set for which the Hausdorff dimension strictly exceeds the topological dimension', which he later retracted and replaced with: 'A fractal is a shape made of parts similar to the whole in some way'. In this book, we will adopt, as a *test for a fractal object, the condition that its fractal dimension exceeds its topological dimension—whichever measure of fractal dimension is employed.* As we do this, bear in mind the ambiguous nature of the definition of a fractal.

2.2—
The Cantor Set

The **Cantor set** must certainly rank as one of the most frequently quoted fractal objects in the literature, alongside perhaps, the Koch curve and Mandelbrot set. It is arguably the simplest of fractals and a good place to begin our discussion on fractals and their geometric properties. The Cantor set consists of an infinite set of disappearing line segments in the unit interval. The best aid to the comprehension of the Cantor set fractal is an illustration of its method of construction. This is given in figure 2.1 for the simplest form of Cantor set, namely the triadic Cantor set. The set is generated by removing the middle third of the unit line segment (step $k = 1$ in the figure). From the two remaining line segments, each one third in length, the middle thirds are again removed (step $k = 2$ in the figure). The middle thirds of the remaining four line segments, each one-ninth in length, are then removed ($k = 3$) and so on to infinity. What is left is a collection of infinitely many disappearing line segments lying on the unit interval whose individual and combined lengths approach zero. This set of 'points' is known as a Cantor set, Cantor dust, or Cantor discontinuum.
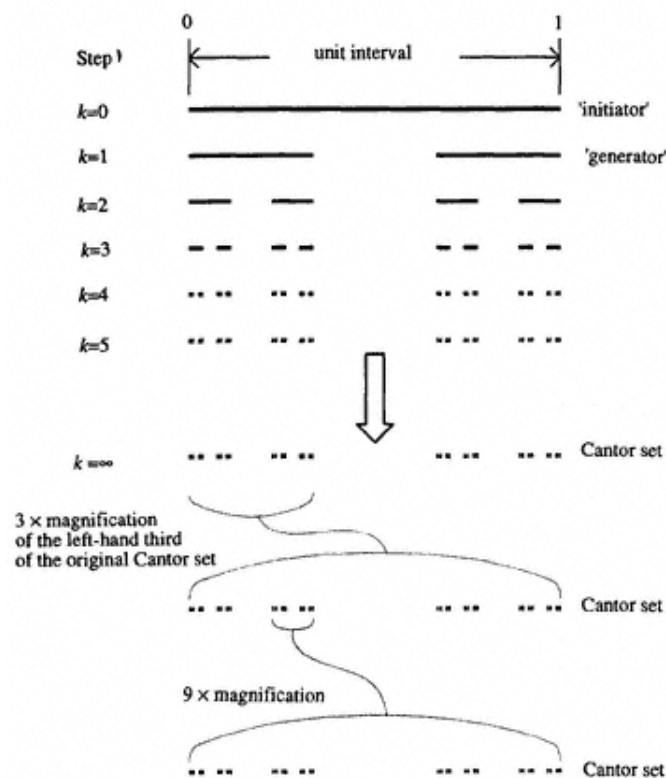
Figure 2.1.
The construction of the triadic Cantor set.

In the construction of the Cantor set the initial unit line segment, $k = 0$, is known as the **initiator** of the set. The first step, $k = 1$, is known as the **generator** (or sometimes motif), as it is the repeated iteration of this step on subsequent line segments which leads to the generation of the set. Notice in the figure that the fifth iteration is indistinguishable from the Cantor set obtained at higher iterations. This problem occurs due to the limit of the finite detail our eyes (or the printer we use to plot the image) can resolve. Thus, to illustrate the set, it is sufficient to repeat the generation process only by the number of steps necessary to fool the eye, and not an infinite number of times. (This is true for all illustrations of fractal objects.) However, make no mistake, only after an infinite number of iterations do we obtain the Cantor set. For a finite number of iterations the object produced is merely a collection of line segments with finite measurable length. These objects formed *en route* to the fractal object are termed **prefractals.**

The Cantor set is a regular fractal object which exhibits exact self-similarity over all scales. This property is illustrated at the bottom of figure 2.1, where the left-hand third of the Cantor set is magnified three times. After magnification we see that the original

Cantor set is formed. Further zooming into one ninth of the newly formed set, we see that again the original set is formed. In fact copies of the Cantor set abound. Zooming into any apparent 'point' in the set produces the original set. It is easily seen that the Cantor set contains an infinite number of copies of itself, within itself, or to put it another way the Cantor set is made up of Cantor sets.
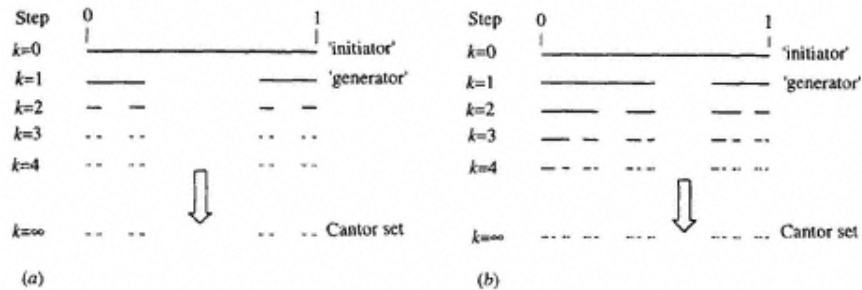

Figure 2.2.
Two more examples of Cantor set construction. (a) Middle half removal. (b) Two-scale Cantor construction.

The triadic Cantor set described above is so called as it involves the removal of the middle third of the remaining line segments at each step in its construction. Any number of variants of the Cantor set may be formed by changing the form of the generator. Two such Cantor sets are shown in figure 2.2. The set on the left of the figure is formed by removing the middle half of each remaining line segment at each step, leaving the end quarters of the line. In the right-hand construction, the segment of each line removed at each stage leaves the first half of the original line and the last quarter. Again after an infinite number of steps a Cantor set is formed.

The Cantor set is simple in its construction, yet it is an object with infinitely rich structure. How do we make sense of the Cantor set? It does not fill up the unit interval continuously, as a line, i.e. one-dimensional object, nor is it a countable collection of zero-dimensional points. Rather, it fills up the unit interval in a special way and as a complete set has a dimension which is neither zero nor one, in fact it has a non-integer, fractal dimension somewhere in between zero and one. Non-integer, fractal dimensions are quite difficult to conceptualize initially and will be dealt with in the following sections.

2.3—
Non-Fractal Dimensions:
The Euclidean and Topological Dimensions.

Generally, we can conceive of objects that are zero dimensional or 0D (points), 1D (lines), 2D (planes), and 3D (solids) see figure 2.3. We feel comfortable with zero, one, two and three dimensions. We form a 3D picture of our world by combining the 2D images from each of our eyes. Is it possible to comprehend higher-dimensional objects, i.e. 4D, 5D, 6D and so on? What about non-integer-dimensional objects such as 2.12D, 3.79D or 36.91232 . . . D?
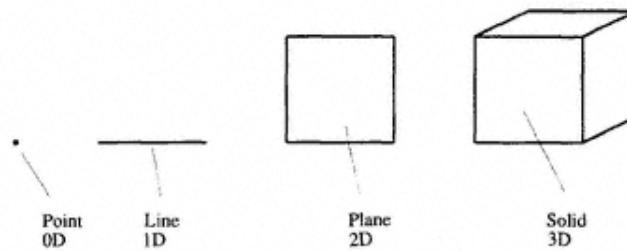
Figure 2.3.
Common integer dimensions.

We will encounter many definitions of dimension as we proceed through this book. Before we deal with fractal dimensions, let us look at the two most common, and perhaps most comprehensible, definitions of dimension, the **Euclidean dimension**, D_E, and **topological dimension,** D_T. Both definitions lead to non-fractal, integer dimensions. The Euclidean dimension is simply the number of co-ordinates required to specify the object. The topological dimension is more involved. The branch of mathematics known as topology considers shape and form of objects from essentially a qualitative point of view. Topology deals with the ways in which objects may be distorted from one shape and formed into another without losing their essential features. Thus straight lines may be transformed into smooth curves or bent into 'crinkly' curves as shown in figure 2.4, where each of the constructions are topologically equivalent. Certain features are invariant under proper transformations (called homeomorphisms by topologists)— for instance, holes in objects remain holes regardless of the amount of stretching and twisting the object undergoes in its transformation from one shape to another. All of the two-holed surfaces in figure 2.5, although quite different in shape, are topologically equivalently as each one may be stretched and moulded into one of the others.

Figure 2.4.
Topologically equivalent curves.

The topological dimension of an object does not change under the transformation of the object. The topological dimension derives from the ability to cover the object with discs of small radius. This is depicted in figure 2.6. The line segment may be covered using many discs intersecting many times with each other (figure 2.6(a)). However, it is possible to refine this covering using discs with only a single intersection between adjacent pairs of discs (figure 2.6(b)). Even when the line is contorted, one can find

Figure 2.5.
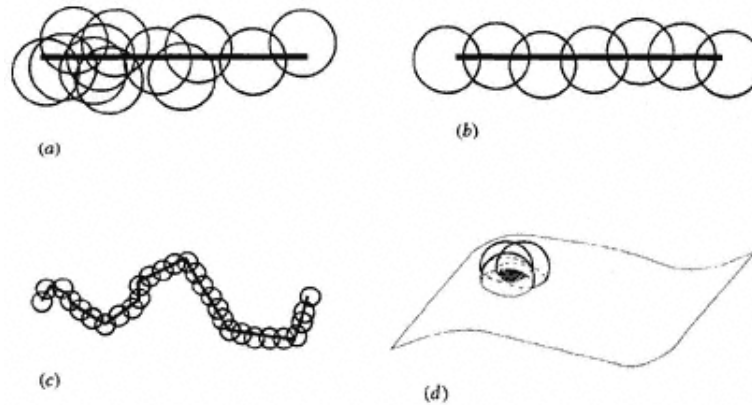Topologically equivalent forms—surfaces with two holes.

Figure 2.6.
The covering of objects with discs and spheres to reveal the topological
dimension. (*a*) Line segment covered by discs. (*b*) Line segment covered by
discs only intersecting in pairs. (*c*) Crinkly line covered by discs only intersecting
in pairs. (*d*) Surface covered by spheres the intersection region is shaded.

discs sufficiently small to cover it with only intersections occurring between adjacent pairs of the covering discs, depicted in figure 2.6(*c*). The segment within each covering disc can itself be covered using smaller discs which require only to intersect in pairs. In a similar manner, a surface may be covered using spheres of small radius with a minimum number of intersections requiring intersecting triplets of spheres (figure 2.6(*d*)). The definition of the topological dimension stems from this observation. The covering of an object by elements (discs or spheres) of small radius requires intersections between a minimum of $D_T + 1$ groups of elements. Figure 2.7 shows a comprehensive set of common forms with their respective Euclidean and topological dimensions. Figure 2.8 contains the Cantor set. Its Euclidean dimension, D_E, is obviously equal to one, as we require one co-ordinate direction to specify all the points on the set. It can be seen from the figure that it is possible to find single non-intersecting discs of smaller and smaller radius to cover sub-elements of the set, thus the topological dimension, D_T, of the Cantor set is zero.
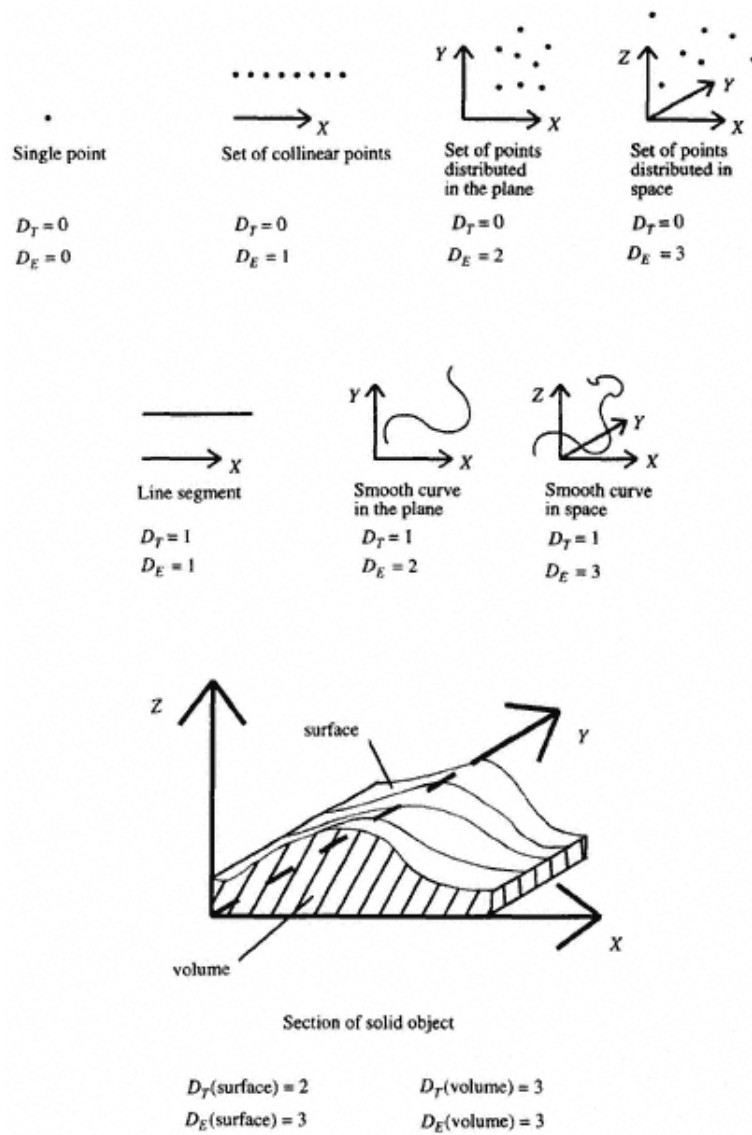
Single point

Set of collinear points

Set of points distributed in the plane

Set of points distributed in space

$D_T = 0$
$D_E = 0$

$D_T = 0$
$D_E = 1$

$D_T = 0$
$D_E = 2$

$D_T = 0$
$D_E = 3$

Line segment

Smooth curve in the plane

Smooth curve in space

$D_T = 1$
$D_E = 1$

$D_T = 1$
$D_E = 2$

$D_T = 1$
$D_E = 3$

surface

volume

Section of solid object

$D_T(\text{surface}) = 2$
$D_E(\text{surface}) = 3$

$D_T(\text{volume}) = 3$
$D_E(\text{volume}) = 3$

Figure 2.7.
A set of common forms with their respective
Euclidean and topological dimensions.
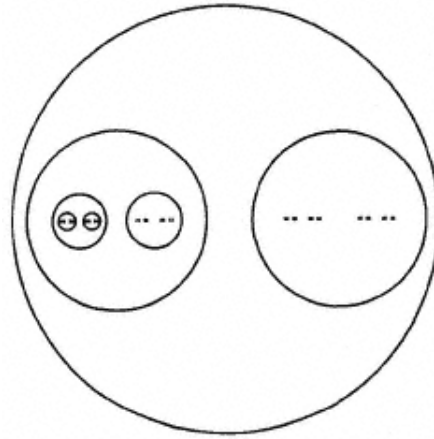
Figure 2.8.
Covering the Cantor set with successively
smaller, non-intersecting discs to reveal
the topological dimension.

2.4—
The Similarity Dimension

Their are many definitions of dimension which give a non-integer, or fractal, dimension. These dimensions are particularly useful in characterizing fractal objects. In the remaining parts of this chapter we will concentrate on the **similarity dimension,** denoted Ds, to characterize the construction of regular fractal objects. As we proceed through subsequent chapters of the text further definitions of dimension will be introduced where appropriate.

The concept of dimension is closely associated with that of scaling. Consider the line, surface and solid depicted in figure 2.9, divided up respectively by self-similar sub-lengths, sub-areas and sub-volumes of side length ε. For simplicity in the following derivation assume that the length, L, area, A, and volume, V, are all equal to unity.

Consider first the line. If the line is divided into N smaller self-similar segments, each ε in length, then ε is in fact the scaling ratio, i.e. $\varepsilon/L = \varepsilon$, since $L = 1$. Thus

$$L = N\varepsilon = 1 \qquad (2.1a)$$

i.e. the unit line is composed of N self-similar parts scaled by $\varepsilon = 1/N$.

Now consider the unit area in figure 2.4. If we divide the area again into N segments each ε^2 in area, then

$$A = N\varepsilon^2 = 1 \qquad (2.1b)$$

i.e. the unit surface is composed of N self-similar parts scaled by $\varepsilon = 1/N^{1/2}$.

Applying similar logic, we obtain for a unit volume

$$V = N\varepsilon^3 = 1 \qquad (2.1c)$$

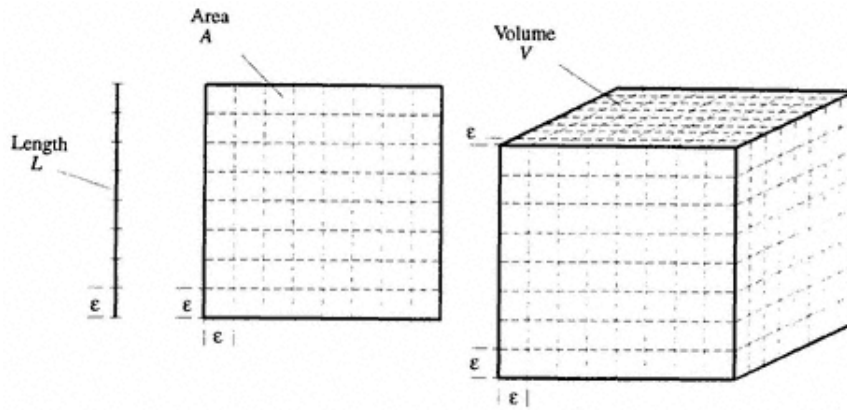i.e. the unit solid is N self-similar parts scaled by $\varepsilon = 1/N^{1/3}$.

Figure 2.9.
Scaling and dimension. Each object consists of N elements of side length ε,
N is determined by the choice of ε. It should be noted that N for each
object need not necessarily be the same, as is the case shown above.

Examining expressions (2.1a–c) we see that the exponent of e in each case is a measure of the (similarity) dimension of the object, and we have in general

$$N\varepsilon^{D_S} = 1. \qquad (2.2)$$

Using logarithms leads to the expression,

$$D_S = \frac{\log(N)}{\log(1/\varepsilon)}. \qquad (2.3)$$

Note that here the subscript 'S' denotes the similarity dimension.

The above expression has been derived using familiar objects which have the same integer Euclidean, topological and similarity dimensions, i.e. a straight line, planar surface and solid object, where $D_E = D_S = D_T$. However, equation (2.3) may also be used to produce dimension estimates of fractal objects where D_S is non-integer. This can be seen by applying the above definition of the self-similar dimension to the triadic Cantor set constructed in section 2.2, (see figures 2.1 and 2.8). From figure 2.1 we saw that the left-hand third of the set contains an identical copy of the set. There are two such identical copies of the set contained within the set, thus $N = 2$ and $\varepsilon = \frac{1}{3}$. According to equation (2.3) the similarity dimension is then

$$D_S = \frac{\log(2)}{\log(1/(1/3))} = \frac{\log(2)}{\log(3)} = 0.6309\ldots. \qquad (2.4a)$$

Thus, for the Cantor set, D_S is less than one and greater than zero: in fact it has a non-integer similarity dimension of 0.6309 . . . due to the fractal structure of the object. We saw in the previous section that the Cantor set has Euclidean dimension of one and a topological dimension of zero, thus $D_E > D_S > D_T$. As the similarity dimension

exceeds the topological dimension, according to our test for a fractal given in section 2.1, the set is a fractal with a fractal dimension defined by the similarity dimension of 0.6309. . . . As an aid to comprehension it may be useful to think of the Cantor set as neither a line nor a point, but rather something in between.

Instead of considering each sub-interval of the Cantor set scaled down by one-third we could have looked at each subinterval scaled down by one-ninth. As we saw from figure 2.1, there are four such segments, each an identical copy of the set. In this case $N = 4$ and $\varepsilon = \frac{1}{9}$ and again this leads to a similarity dimension of

$$D_S = \frac{\log(4)}{\log\left(1/(1/9)\right)} = \frac{\log(4)}{\log(9)} = \frac{2\log(2)}{2\log(3)} = 0.6309\ldots. \qquad (2.4b)$$

Similarly there are eight smaller subintervals containing identical copies of the set each at a scale of 2 of the original set, giving

$$D_S = \frac{\log(8)}{\log\left(1/(1/27)\right)} = \frac{\log(8)}{\log(27)} = \frac{3\log(2)}{3\log(3)} = 0.6309\ldots \qquad (2.4c)$$

and so on.

By now a general scaling rule is apparent. The general expression for the similarity dimension of the Cantor set is

$$D_S = \frac{\log(2^C)}{\log(3^C)} = \frac{C\log(2)}{C\log(3)} = \frac{\log(2)}{\log(3)} = 0.6309\ldots \qquad (2.4d)$$

where the scaling constant, C, depends on the scale used to identify the self-similarity of the object. It can be seen from the above that the similarity dimension is independent of the scale used to investigate the object.

2.5—
The Koch Curve

The **Koch curve,** the method of construction of which is illustrated in figure 2.10, is another well documented fractal. As with the Cantor set, the Koch curve is simply constructed using an iterative procedure beginning with the initiator of the set as the unit line segment (step $k = 0$ in the figure). The unit line segment is divided into thirds, and the middle third removed. The middle third is then replaced with two equal segments, both one-third in length, which form an equilateral triangle (step $k = 1$): this step is the generator of the curve. At the next step ($k = 2$), the middle third is removed from each of the four segments and each is replaced with two equal segments as before. This process is repeated an infinite number of times to produce the Koch curve. Once again the self-similarity of the set is evident: each sub-segment is an exact replica of the original curve, as shown in figure 2.11.

A noticeable property of the Koch curve is that it is seemingly infinite in length. This may be seen from the construction process. At each step, k, in its generation, the length of the prefractal curve increases to $\frac{4}{3}L_{k-1}$, where L_{k-1} is the length of the curve in the preceding step. As the number of generations increase the length of the curve diverges. It is therefore apparent that length is not a useful measure of the Koch curve, as
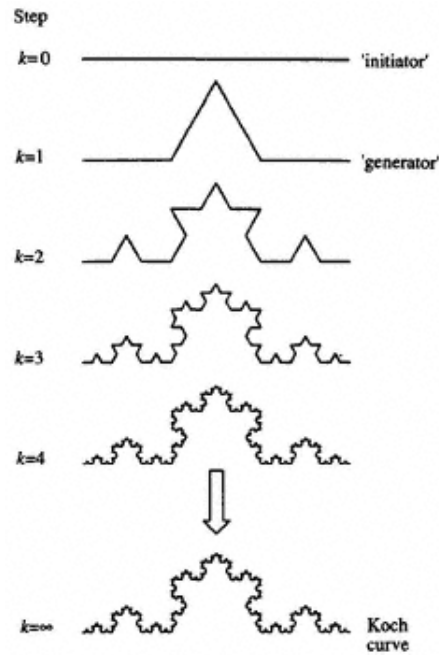
Figure 2.10.
The construction of the Koch curve.

defined in the limit of an infinite number of iterations. In addition, it can be shown that the Koch curve is effectively constructed from corners, hence no unique tangent occurs anywhere upon it. The Koch curve is not a smooth curve and is nowhere-differentiable, as a unique tangent, or slope, cannot be found anywhere upon it.

The Koch curve is a fractal object possessing a fractal dimension. Each smaller segment of the Koch curve is an exact replica of the whole curve. As we can see from figure 2.11, at each scale there are four sub-segments making up the curve, each one a one third reduction of the original curve. Thus, $N = 4$, $\varepsilon = \frac{1}{3}$, and the similarity dimension based on expression (2.3) is

$$D_S = \frac{\log(N)}{\log(1/\varepsilon)} = \frac{\log(4)}{\log(3)} = 1.2618\ldots \qquad (2.5)$$

that is, the Koch curve has a dimension greater than that of the unit line ($D_E = D_T = 1$) and less than that of the unit area ($D_E = D_T = 2$). The Euclidean dimension of the Koch curve, D_E, is two as we need two co-ordinate directions to specify all points on it. The topological dimension, D_T, of the Koch curve is unity , as we can cover it with successively smaller discs intersecting in pairs. The similarity dimension of the Koch curve lies between its Euclidean and topological dimension, i.e. $D_E > D_S > D_T$, which leads us to conclude that it is indeed a fractal object, with a fractal (similarity) dimension, D_S, of 1.2618 . . . .
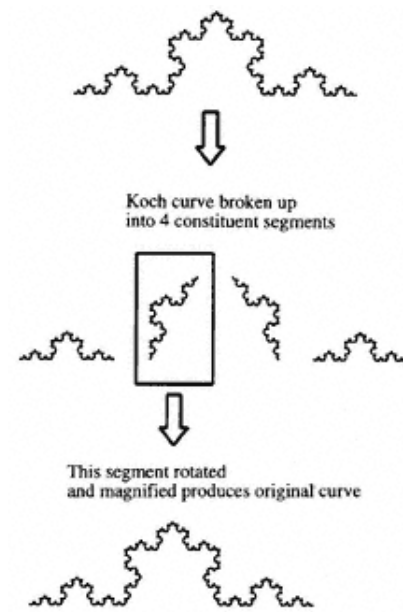
Koch curve broken up
into 4 constituent segments

This segment rotated
and magnified produces original curve

Figure 2.11.
The self-similar structure of the Koch curve.

Step

$k = 0$ 'initiator'
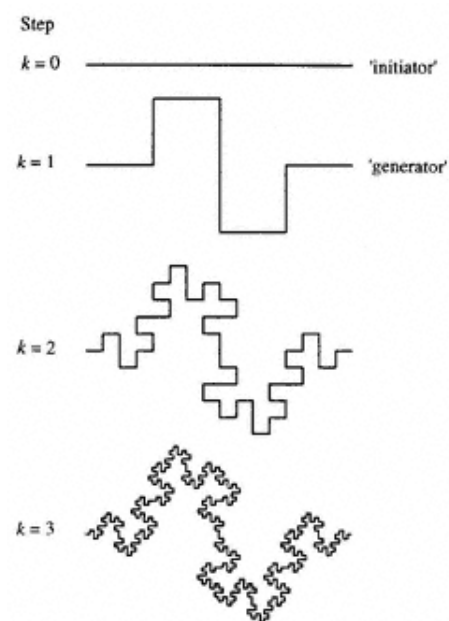
$k = 1$ 'generator'

$k = 2$

$k = 3$

Figure 2.12.
The first three stages in the
construction of the quadratic Koch curve.

2.6—
The Quadratic Koch Curve

The Koch curve shown in both figures 2.10 and 2.11 is more specifically known as the triadic Koch curve. As with the triadic Cantor set, the triadic Koch curve's name stems from the fact that the middle thirds of the line segments are modified at each step. By changing the form of the generator a variety of Koch curves may be produced. Figure 2.12 contains the first three stages in the construction of the quadratic Koch curve, also known as the Minkowski sausage. This curve is generated by repeatedly replacing each line segment, composed of four quarters, with the generator consisting of eight pieces, each one quarter long (see figure 2.12). As with the triadic Koch curve the Minkowski sausage is a fractal object. Each smaller segment of the curve is an exact replica of the whole curve. There are eight such segments making up the curve, each one a one-quarter reduction of the original curve. Thus, $N = 8$, $\varepsilon = \frac{1}{4}$, and the similarity dimension based on expression (2.3) is

$$D_S = \frac{\log(N)}{\log(1/\varepsilon)} = \frac{\log(8)}{\log(4)} = \frac{3\log(2)}{2\log(2)} = \frac{3}{2} = 1.5. \qquad (2.6)$$

Figure 2.13 contains four more Koch curves produced using a variety of generators. The reader is invited to define his, or her, own generators, and use them to produce new fractal curves.
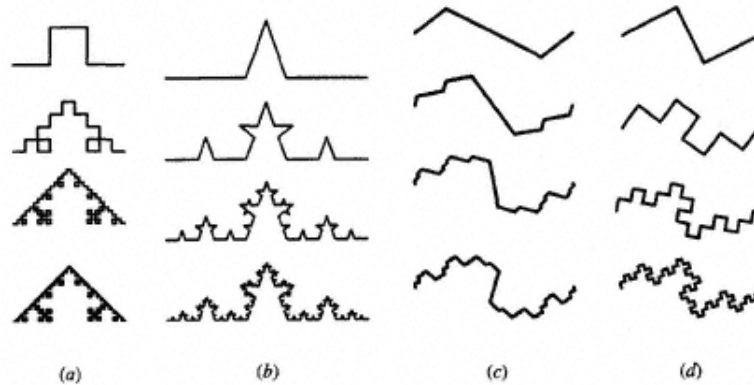

Figure 2.13.
Miscellaneous Koch curve constructions (all have unit line initiators—not shown).

2.7—
The Koch Island

The Koch island (or snowflake) is composed of three Koch curves rotated by suitable angles and fitted together: its construction is shown in figure 2.14. We already know that the length of the Koch curve is immeasurable, so the length of the coastline of the Koch island is seemingly infinite, but what about the area bounded by the perimeter of the island? It certainly looks finite. We can obtain a value for the bounded area by examining the construction process. Let us first assume for simplicity that the initiator is
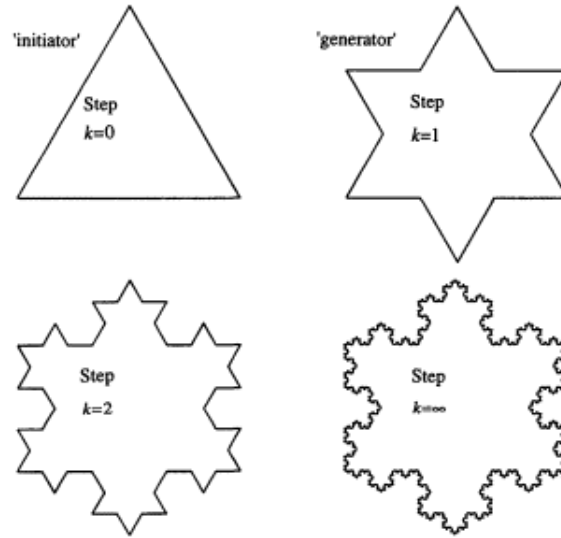
Figure 2.14.
The Koch island and its construction.

composed of three unit lines. The area bounded by the perimeter is then half of the base multiplied by the height of the equilateral triangle, i.e. $\frac{1}{2} \times 1 \times \sqrt{3}/2$. At step $k = 1$ three smaller triangles are added, each with a base length equal to one third. At step $k = 2$ another twelve smaller triangles are added, each with base length equal to one ninth. At step $k = 3$ (not shown in the figure) forty-eight smaller triangles are added, each with base length of one twenty-seventh. The area then increases at each stage as follows:

$$\text{step } k = 0 \quad \text{area} = \frac{1}{2} \times \frac{\sqrt{3}}{2} \times 1 = \frac{\sqrt{3}}{4} \qquad (2.7a)$$

$$\text{step } k = 1 \quad \text{area} = \frac{\sqrt{3}}{4} + 3\left(\frac{\sqrt{3}}{4 \times 3} \times \frac{1}{3}\right) \qquad (2.7b)$$

$$\text{step } k = 2 \quad \text{area} = \frac{\sqrt{3}}{4} + 3\left(\frac{\sqrt{3}}{4 \times 3} \times \frac{1}{3}\right) + 12\left(\frac{\sqrt{3}}{4 \times 9} \times \frac{1}{9}\right) \qquad (2.7c)$$

$$\text{step } k = 3 \quad \text{area} = \frac{\sqrt{3}}{4} + 3\left(\frac{\sqrt{3}}{4 \times 3} \times \frac{1}{3}\right)$$

$$+ 12\left(\frac{\sqrt{3}}{4 \times 9} \times \frac{1}{9}\right) + 48\left(\frac{\sqrt{3}}{4 \times 27} \times \frac{1}{27}\right) \qquad (2.7d)$$

In general, for an arbitrary step k

$$\text{Area} = \frac{3 \times \sqrt{3}}{4 \times 4}\left(\frac{4}{3} + \frac{4^1}{9^1} + \frac{4^2}{9^2} + \frac{4^3}{9^3} + \ldots + \frac{4^k}{9^k}\right). \qquad (2.7e)$$

We may then split up this expression to give

$$\text{area} = \frac{3 \times \sqrt{3}}{16}\left(\frac{1}{3}\right) + \frac{3 \times \sqrt{3}}{16}\left(1 + \frac{4^1}{9^1} + \frac{4^2}{9^2} + \frac{4^3}{9^3} + \dots + \frac{4^k}{9^k}\right). \qquad (2.7f)$$

In the limit, as k tends to infinity, the geometric series in the brackets on the right-hand side of the above expression tends to $\frac{9}{5}$: this leaves us with an area of

$$\text{area} = \frac{3 \times \sqrt{3}}{16}\left(\frac{1}{3} + \frac{9}{5}\right) = \frac{3 \times \sqrt{3}}{16} \times \frac{32}{15} = \frac{2}{5}\sqrt{3}. \qquad (2.7g)$$

The Koch island therefore has a finite area of $\frac{2}{5}\sqrt{3}$, or about 0.693 units (of area). Thus, the Koch island has a regular area, in the sense that it is bounded and measurable, but an irregular, immeasurable perimeter. To generate the Koch island, we used three Koch curves with unit initiator. However, if the initiator were a in length, then the area would be simply $\frac{2}{5}\sqrt{3}a^2$. You can easily verify this for yourself. We will return briefly to the Koch island in our discussion of the fractal nature of natural coastlines in the next chapter.
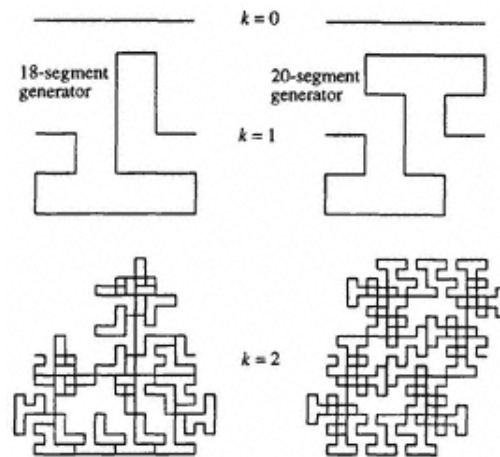

Figure 2.15.
The construction process for curves with
similarity dimension greater than two.

2.8—
Curves in the Plane with Similarity Dimension Exceeding Two

The similarity dimension can exceed two for curves in the plane. This may initially seem counter-intuitive, however, it may be easily demonstrated. Figure 2.15 contains two curves whose generators replace the original line segments with curves consisting of eighteen and twenty segments respectively, each of side length one quarter of the original. The similarity dimension of the curve resulting from the eighteen-segment generator is

$$D_S = \frac{\log(N)}{\log(1/\varepsilon)} = \frac{\log(18)}{\log(4)} = 2.0849\dots. \qquad (2.8)$$

Similarly, $D_S = 2.1609\ldots$ for the twenty-segment curve. The similarity dimension exceeds two in these cases due to the overlapping parts of the fractal curve. Here, for both curves we have the slightly unusual condition that $D_S > D_E > D_T$, however, as the fractal dimension exceeds the topological dimension the object is still fractal by our definition. One way to avoid the fractal dimension exceeding D_E is to use alternative definitions of dimension which only count overlapping parts of the curve once. These will be explored in the next chapter.
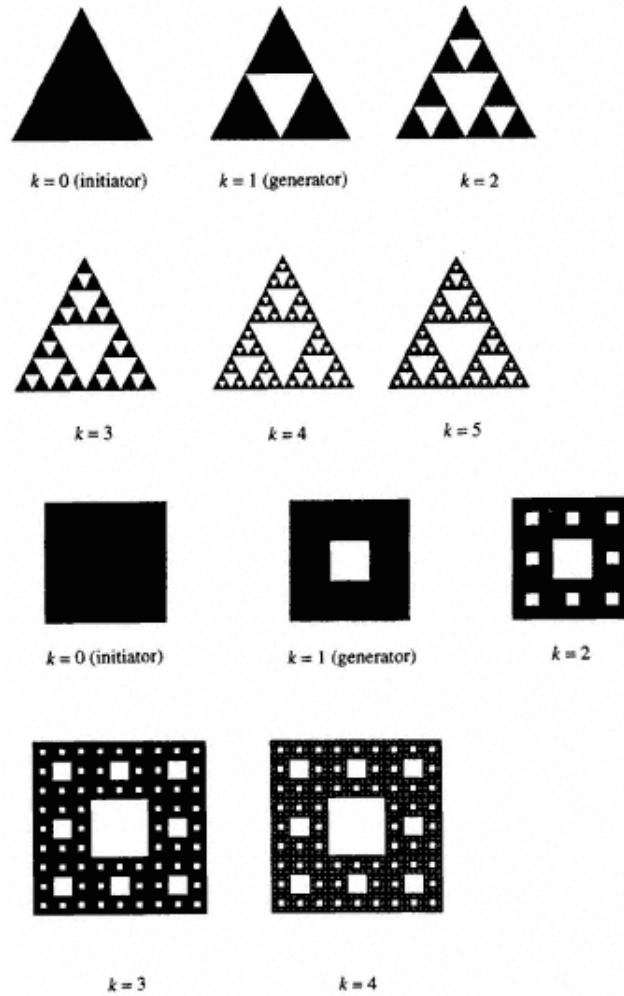

Figure 2.16.
Construction of the Sierpinski gasket (top) and carpet (bottom).

2.9—
The Sierpinski Gasket and Carpet

The construction of the **Sierpinski gasket** is illustrated in figure 2.16. The initiator in this case is a filled triangle in the plane. The middle triangular section is removed from the original triangle. Then the middle triangular sections are removed from the remaining triangular elements and so on. After infinite iterations the Sierpinski gasket is formed. Each prefractal stage in the construction is composed of three smaller copies of the preceding stage, each copy scaled by a factor of one half. The similarity dimension is given by

$$D_S = \frac{\log(N)}{\log(1/\varepsilon)} = \frac{\log(3)}{\log(2)} = 1.5849\dots. \tag{2.9}$$

A sister curve to the Sierpinski gasket is the **Sierpinski carpet** also shown in figure 2.16. Its method of construction is similar to that of the gasket: this time the initiator is a square and the generator removes the middle square, side length one-third, of the original square. With both the Sierpinski gasket and carpet, the constructions lead to fractal curves whose area vanishes.
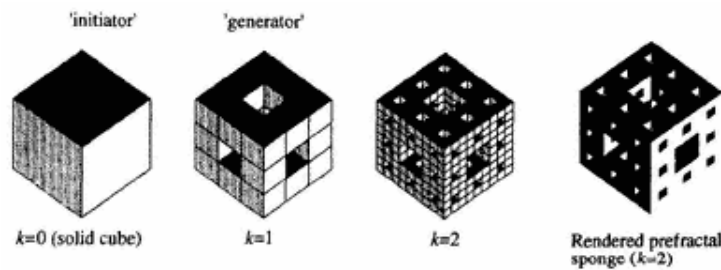

Figure 2.17.
Constructing the Menger sponge.

2.10—
The Menger Sponge.

So far we have looked at constructions on the line (Cantor set) and in the plane (Koch curve and Sierpinski gasket and carpet). We end this chapter with an interesting object constructed in 3D space—the **Menger sponge.** Its construction is shown in figure 2.17 and, as can be seen, it is closely related to the Sierpinski carpet. The initiator in the construction is a cube. The first iteration towards the final fractal object, the generator, is formed by 'drilling through' the middle segment of each face. This leaves a prefractal composed of twenty smaller cubes each scaled down by one-third. These cubes are then drilled out leaving 400 cubes scaled down by one-ninth from the original cube (step $k = 2$ in the figure). Repeated iteration of this construction process leads to the Menger sponge. The similarity dimension of the Menger sponge is

$$D_S = \frac{\log(N)}{\log(1/\varepsilon)} = \frac{\log(20)}{\log(3)} = 2.7268\dots \tag{2.10}$$

which is between its topological dimension of one (as it is a curve with zero volume, zero area and infinite length) and Euclidean dimension of three.

2.11—
Chapter Summary and Further Reading

2.11.1—
Chapter Keywords and Key Phrases

exact self-similarity	*regular fractals*	*fractal dimension*
Cantor set	*initiator*	*generator*
prefractals	*Euclidean dimension*	*topological dimension*
similarity dimension	*Koch curve*	*Sierpinski gasket/carpet*
Menger sponge		

2.11.2—
Summary and Further Reading

In this chapter we have been introduced to regular fractal objects which have exact self-similarity at all scales, i.e. each small part of the object contains identical copies of the whole. To characterize these fractals requires that we re-evaluate our concepts of dimension. The Euclidean and topological definitions of dimension give only integer values. To obtain a fractal dimension for the exactly self-similar fractals we used, possibly the simplest definition of fractal dimension, the similarity dimension, D_S. In general, if the similarity dimension is greater than the topological dimension of the object then the object is a fractal, and, more often than not, the fractal dimension is a non-integer value. For more examples and information on exactly self-similar fractals the reader is referred for an elementary introduction to the book by Lauwerier (1991), and for an intermediate and comprehensive introduction to the book by Mandelbrot (1977), or, better, the extended version of this text by Mandelbrot (1982a). In-depth accounts of the Cantor set, Koch curve, Sierpinski gasket and Menger sponge, together with brief biographical details of their originators, are given by Peitgen *et al* (1992a). A method for the generation of the Sierpinski gasket using random numbers is given, amongst other useful information, by Peitgen *et al* (1991). Reiter (1994) presents some computer generated generalizations of the Sierpinski gaskets and carpets and the Menger sponge. The computer generation of the Koch curve is discussed by Hwang and Yang (1993). David (1995) presents two examples of 3D regular fractals based on Keplerian solids and Wicks (1991) presents an advanced mathematical account of fractals and hyperspaces.

Much of the interest in fractal geometry lies in its ability to describe many natural objects and processes, however, generally these are not exactly self-similar but rather statistically self-similar, whereby each small part of the fractal has the same statistical properties as the whole. We move on to these statistical, or random, fractals in the following chapter.

2.12—
Revision Questions and Further Tasks

Q2.1 List the keywords and key phrases of this chapter and briefly jot down your

understanding of them.

Q2.2 Sketch out a line of unit length and plane of unit area. By selecting appropriate self-similar parts find their Euclidean, topological, and similarity dimensions, and show that they are not fractal objects.

Q2.3 (*a*) What are the Euclidean and topological dimensions of the Koch curve constructions shown in figure 2.13?

(*b*) Assuming that the line segments of the generator in figure 2.13(*a*) are all the same length, calculate the similarity dimension of the resulting fractal curve.

(*c*) The lengths of the line segments in the generator of figure 2.13(*d*) are each one half of the original unit line initiator. What is the similarity dimension of the resulting fractal curve?

(*d*) Try to produce some of your own Koch curves and find their similarity dimension.
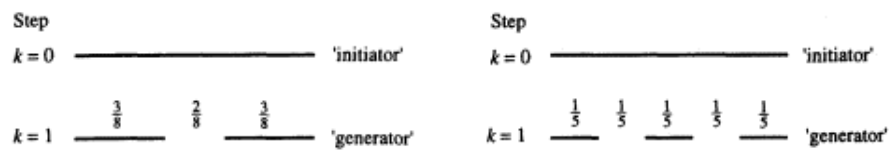

Figure Q2.4.
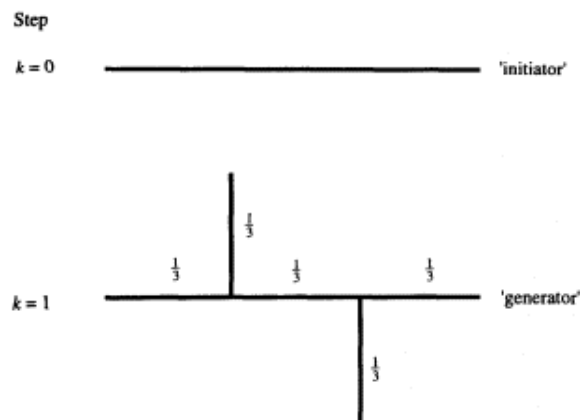The initiator and generator for two Cantor sets.

Figure Q2.5.
The initiator and generator of a fractal curve.

Q2.4 The initiator and generator of two Cantor sets are given above in figure Q2.4. On graph paper generate the first four prefractals of the set. What is the similarity dimension of the resulting Cantor sets after infinite repetitions of the construction process?

Q2.5 The initiator and generator of a fractal curve are given in figure Q2.5. On graph paper generate the first few (as many as you can) prefractals of the set. What is the similarity dimension of the resulting fractal curve after infinite repetitions of the construction process?

Q2.6 (*a*) Show that the similarity dimension of the fractal curve on the right-hand side of figure 2.15 is greater than two.

(*b*) Explain why a curve generated in the plane can have a similarity dimension exceeding 2.

(*c*) Try to produce your own curves with $D_S > 2$.

Q2.7 What is the similarity dimension of the Sierpinski carpet shown in figure 2.16?
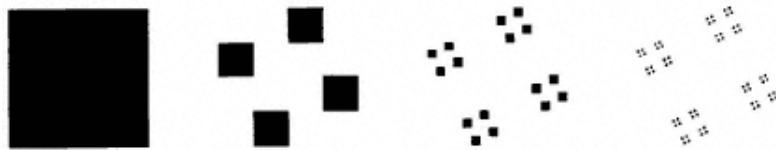

Figure Q2.8.
The construction of a fractal dust.

Q2.8 The generation process of a fractal dust is given in figure Q2.8. At each stage the remaining squares are divided into sixteen smaller squares and twelve of them removed. What is the resulting self-similarity dimension of the dust? What is the topological and Euclidean dimension of the dust? Explain why it is a fractal object.

Q2.9 (*a*) Generate the $k = 3$ iteration of a quadratic Koch island. Use the unit square as the initiator and the construction given in figure 2.12 to generate the curve on each of the four initiators.

(*b*) What is the area of the quadratic Koch island?

(*c*) If the initiator were a square of side length a, what would the resulting area of the Koch island be?

Chapter 3—
Random Fractals

3.1—
Introduction

In chapter 2 we investigated the properties of regular fractals—regular in the sense that they are composed of scaled down and rotated <u>identical</u> copies of themselves. The exact structure of regular fractals is repeated within each small fraction of the whole, i.e. they are exactly self-similar. There is, however, another group of fractals, known as **random fractals,** which contain a random or statistical element. These fractals are not exactly self-similar, but rather **statistically self-similar.** Each small part of a random fractal has the same statistical properties as the whole. Random fractals are particularly useful in describing the properties of many natural objects and processes.

3.2—
Randomizing the Cantor Set and Koch Curve.

A simple way to generate a fractal with an element of randomness is to add some probabilistic element to the construction process of a regular fractal, such as those investigated in chapter 2. A random version of the Cantor set may be produced in several ways, and figure 3.1 illustrates two methods for producing random Cantor sets. In the method depicted at the top of figure 3.1, the triadic Cantor set construction process is modified to allow the removal of <u>any</u> one third of each line segment at each prefractal stage. The third to be removed is selected at random. The generation of the set at the bottom of figure 3.1 again shows a random generation of a Cantor set, this time each remaining line segment is replaced with two smaller segments of random length. As we zoom into each of these Cantor sets we find that they have a statistical self-similarity as their construction involves the same random process at all scales.

Figure 3.2 illustrates the construction of a random version of the Koch curve. Its construction is very similar to that of the triadic Koch curve, investigated in chapter 2, in that the generation process involves the removal of the middle third of the remaining line segments at each prefractal stage, replacing the removed segment with two sides of an equilateral triangle. This time, however, the replacement elements are randomly placed either side of the removed segment. The resulting random fractal curve looks rather irregular compared to its cousin, the exactly self-similar triadic Koch curve of figure 2.10. As with its regular counterpart, any attempt to measure the length of the random
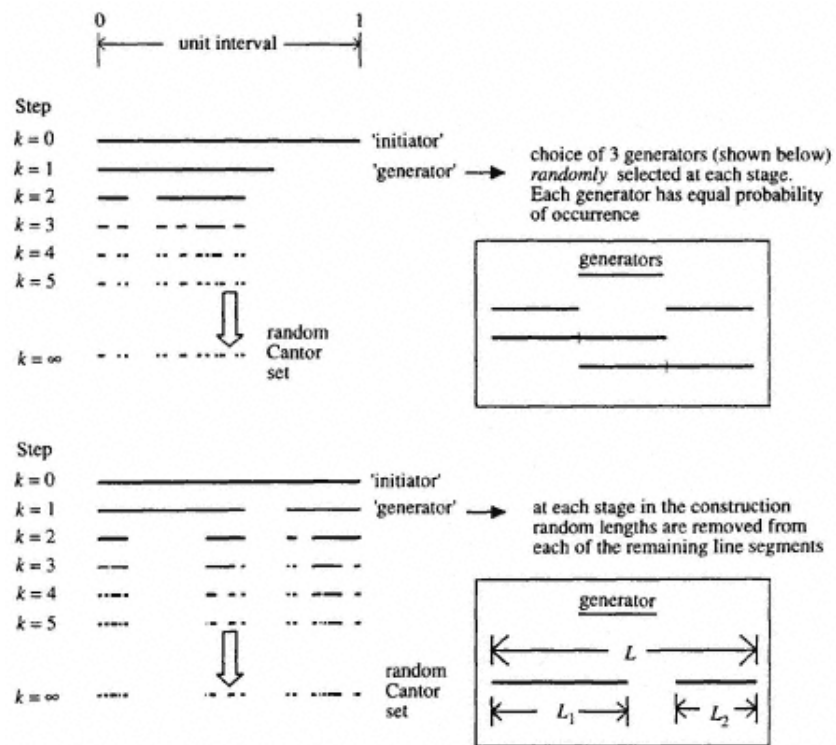
Figure 3.1.
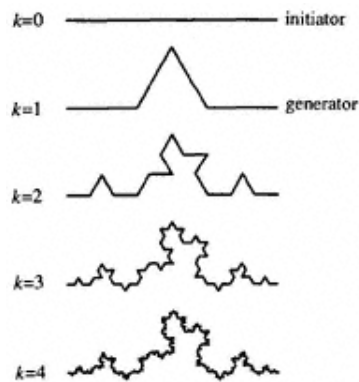Two methods for randomizing the Cantor set.

Figure 3.2.
The first four steps in the construction
of the randomized Koch curve.

Koch curve is futile as the measurement diverges with each iteration. However, the random Koch curve still retains a degree of regularity as, at each stage in the construction process, regular triangular features are placed randomly either side of the removed line segment.

3.3—
Fractal Boundaries

A fractal boundary is a non-crossing fractal curve which reveals more structure as one zooms in. The Koch island investigated in chapter 2 (figure 2.14) had a boundary, or coastline, consisting of three Koch curves, i.e. it had a regular fractal boundary. Real coastlines also tend to appear rather rugged at all levels of magnification: this is shown schematically in figure 3.3. However, unlike the coastline of the Koch island a real coastline is statistically self-similar in that randomly selected segments of the coastline possess the same statistical properties over all scales of magnification. Coastlines are, then, random fractal curves.
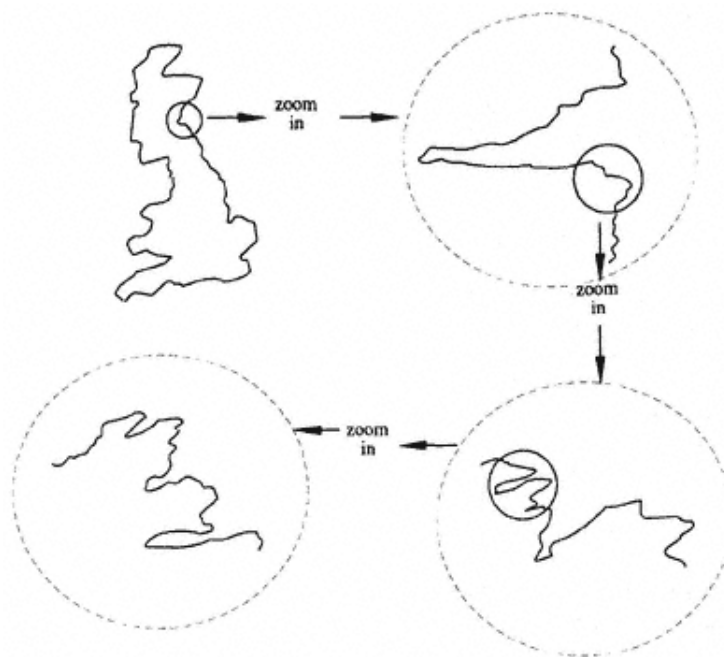

Figure 3.3.
Zooming into a coastline to reveal more structure.

It is worthwhile, at this stage, to restate (see chapter 1) that even the best examples of natural fractals, including coastlines, possess self-similarity over a finite range of scales. This range is, however, sufficiently large to allow fractal geometry to play an important role in their characterization. We will come back to this point when discussing the typical regions of the Richardson plot later in the chapter.

The use of a dimension measurement is a good way to characterize and quantify the statistical self-similarity property of random fractal boundaries. We will not use the similarity dimension defined in chapter 2 as it relies on the identification of exactly self-similar parts at different scales of magnification to produce the dimension measurement. Random fractals do not possess exactly self-similar parts with which to indicate the scaling of the object, hence we need other methods to characterize their scaling properties. Two estimates of the fractal dimension of random coastline fractals which are commonly employed are the **box counting method** and the **structured walk technique.** These are examined in detail in the following sections.

3.4—
The Box Counting Dimension and the Hausdorff Dimension

In chapter 2 we looked at the Euclidean and topological dimensions, both of which are integer dimensions. In addition, we used the similarity dimension to produce fractal dimensions for fractal objects. There are, however, many more definitions of dimension which produce fractal dimensions. One of the most important in classifying fractals is the **Hausdorff dimension.** In fact, Mandelbrot suggested that a fractal may be defined as an object which has a Hausdorff dimension which exceeds its topological dimension. A complete mathematical description of the Hausdorff dimension is outside the scope of this text. In addition, the Hausdorff dimension is not particularly useful to the engineer or scientist hoping to quantify a fractal object, the problem being that it is practically impossible to calculate it for real data. We therefore begin this section by concentrating on the closely related **box counting dimension** and its application to determining the fractal dimension of natural fractals before coming to a brief explanation of the Hausdorff dimension.

(i) *The box counting dimension.* To examine a suspected fractal object for its box counting dimension we cover the object with covering elements or 'boxes' of side length δ. The number of boxes, N, required to cover the object is related to δ through its box counting dimension, D_B. The method for determining D_B is illustrated in the simple example of figure 3.4, where a straight line (a one-dimensional object) of unit length is probed by cubes (3D objects) of side length δ. We require N cubes (volume δ^3) to cover the line. Similarly, if we had used squares of side length δ (area δ^2) or line segments (length δ^1), we would again have required N of them to cover the line. Equally, we could also have used 4D, 5D, or 6D elements to cover the line segment and still required just N of them. In fact, to cover the unit line segment, we may use any elements with dimension greater than or equal to the dimension of the line itself, namely one. To simplify matters, the line in figure 3.4 is specified as exactly one unit in length. The number of cubes, squares or line segments we require to cover this unit line is then $N\delta(=1)$, hence $N = 1/\delta^1$. Notice that the exponent of δ remains equal to one regardless of the dimension of the probing elements, and is in fact the box counting dimension, D_B, of the object under investigation. Notice also that for the unit (straight) line $D_E = D_B = D_T (=1)$, hence it is not a fractal by our definition in section 2.1, as the fractal dimension, here given by D_B, does not exceed the topological dimension, D_T.

To generalize the above and aid in the following discussion it is useful if, at this point, we rename all covering elements as hypercubes, as follows:
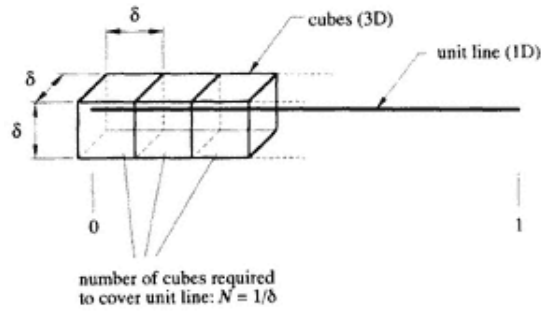
Figure 3.4.
A line (1D) probed using boxes (3D).

1D hypercube = 1D element, i.e. a line segment
2D hypercube = 2D element, i.e. a square
3D hypercube = 3D element, i.e. a box or cube
4D hypercube = 4D element
5D hypercube = 5D element
etc

and similarly rename all measurements as hypervolumes, V^*, as follows:

volume of 1D hypercube = 1D hypervolume (length)
volume of 2D hypercube = 2D hypervolume (area)
volume of 3D hypercube = 3D hypervolume (volume)
volume of 4D hypercube = 4D hypervolume
volume of 5D hypercube = 5D hypervolume
etc.

If we repeat the covering procedure outlined above for a plane unit area, it is easy to see that to cover such a unit area we would require $N = 1/\delta^2$ hypercubes of edge length δ and Euclidean dimension greater than or equal to two. Similarly, with a 3D solid object we would require $N = 1/\delta^3$ hypercubes of edge length δ with Euclidean dimension greater than or equal to three to cover it. Again notice that in each case the exponent of δ is a measure of the dimension of the object. In general, we require $N = 1/\delta^{D_B}$ boxes to cover an object where the exponent D_B is the box counting dimension of the object. We arrive at the following general formulation of D_B for objects of unit hypervolume:

$$D_B = \frac{\log(N)}{\log(1/\delta)} \qquad (3.1)$$

obtained by covering the object with N hypercubes of side length δ. Note that the above expression is of rather limited use. It assumes the object is of unit hypervolume and in general will produce erroneous results for large δ. More general and practically useful expressions are given below in equations (3.4a, b). Note also the marked resemblance of equation (3.1) to the definition of the similarity dimension D_S given in equation (2.3).

However, do not confuse the two: the calculation of D_S requires that exactly self-similar parts of the fractal are identified, whereas D_B requires the object to be covered with self-similar boxes. Hence, D_B allows us greater flexibility in the type of fractal object that may be investigated.
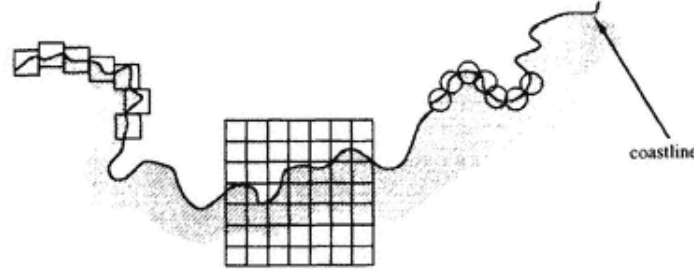

Figure 3.5.
Determining the fractal dimension of a
coastline using the box counting method.

The general expression for the dimension of an object with a hypervolume (i.e. length, area, volume or fractal hypervolume) not equal to unity, but rather given by V^*, is

$$D_B = \frac{\log(N) - \log(V^*)}{\log(1/\delta)} \qquad (3.2)$$

where N is the number of hypercubes of side length δ required to cover the object, i.e. $N = V^*/\delta^{D_B}$. Rearranging equation (3.2) gives

$$\log(N) = D_B \log(1/\delta) + \log(V^*) \qquad (3.3)$$

which is in the form of the equation of a straight line where the gradient of the line, D_B, is the box counting dimension of the object. This form is suitable for determining the box counting dimension of a wide variety of fractal objects by plotting $\log(N)$ against $\log(1/\delta)$ for probing elements of various side lengths, δ. Figure 3.5 illustrates three popular methods of covering a coastline curve using boxes and circles to obtain a box counting dimension estimate. One may place boxes against each other to obtain the minimum number required to cover the curve. Alternatively, one may use a regular grid of boxes and count the number of boxes, N, which contain a part of the curve for each box side length δ. Circles of diameter δ may also be used as probing elements to cover the curve, placing them so that they produce the minimum covering of the curve. In this case, δ corresponds to the diameter of the covering circles. Whichever method is used, we obtain the box counting dimension from the limiting gradient (as δ tends to zero) of a plot of $\log(N)$ against $\log(1/\delta)$, i.e. the derivative

$$D_B = \lim_{\delta \to 0} \frac{d(\log(N))}{d((\log(1/\delta))}. \qquad (3.4a)$$

This is shown schematically in figure 3.6. In practice, the box counting dimension may be estimated by selecting two sets of [$\log(1/\delta)$ $\log(N)$] co-ordinates at small values of δ

(i.e. large values of $\log(1/\delta)$). An estimate of D_B is then given by

$$D_B = \frac{\log(N_2) - \log(N_1)}{\log(1/\delta_2) - \log(1/\delta_1)} \qquad (3.4b)$$
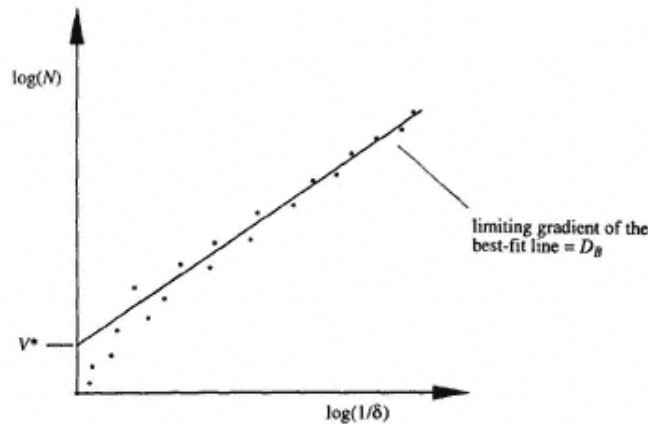

Figure 3.6.
Estimating the box counting dimension of experimental data.

Alternatively, a more refined estimate may be obtained by drawing a best fit line through the points at small values of δ and calculating the slope of this line (see figure 3.6). For this case the N and δ values of equation (3.4b) are taken from two points on the best-fit line. This is particularly advisable where the data fluctuate at the limits of resolution.

The box counting dimension is widely used in practice for estimating the dimension of a variety of fractal objects. The technique is not confined to estimating the dimensions of objects in the plane, such as the coastline curve. It may be extended to probe fractal objects of high fractal dimension in multi-dimensional spaces, using multi-dimensional covering hypercubes. Its popularity stems from the relative ease by which it may be incorporated into computer algorithms for numerical investigations of fractal data. The grid method (central method depicted in figure 3.5) lends itself particularly to encoding within a computer program. By covering the data with grids of different box side lengths, δ, and counting the number of boxes, N, that contain the data, the box counting dimension is easily computed using equation (3.4b). We shall return to the box counting dimension in chapter 7 where we shall investigate its usefulness in characterizing fractal properties of structures associated with chaotic motion in multi-dimensional phase spaces.

(ii) *Hausdorff dimension.* There is a marked similarity between the box counting dimension and the Hausdorff dimension. Both use elements to cover the object under inspection. The difference between the two is really this. When using the box counting dimension we are asking, 'How many boxes or hypercubes do we need to <u>cover</u> the object?': in this case we only need use probing elements, or hypercubes, which have an integer dimension equal to or exceeding that of the object. In contrast, when using

the Hausdorff dimension we are asking instead, 'What is the 'size' of the object?', that is we are trying to <u>measure</u> it. To measure its size or hypervolume we need to use the appropriate dimension of covering hypercubes, this appropriate dimension being the Hausdorff dimension D_H. In the rest of this section a brief overview of the Hausdorff dimension is given for completeness of the text.
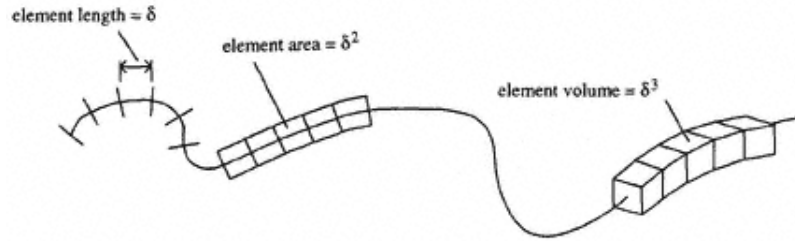

Figure 3.7.
Measuring a smooth curve.

Let us first consider regular, non-fractal, or Euclidean objects. If we want to measure the size of an object we must use a measurement appropriate to its dimension, i.e. length is the natural measure of a line, area is the natural measure of a surface, and volume is the natural measure of a solid. Consider first the measurement of the smooth curve in figure 3.7. To measure the curve we can cover it with measuring elements such as lines, squares or cubes of linear size, δ, as shown in the figure. The length, area and volume of these measuring elements is given by δ^1, δ^2, δ^3 respectively, or more generally given by δ^{D_E} where D_E is the integer Euclidean dimension of the measuring elements.

As with the box counting dimension we require N elements of side length δ to cover the curve. The measured length of the line, as measured by the covering elements, is given by

$$L_m = N\delta^1. \qquad (3.5a)$$

As δ goes to zero in the limit, the measured length, L_m, tends to the true length of the curve L, i.e.

$$L_m \xrightarrow[\delta \to 0]{} L. \qquad (3.5b)$$

Now consider the covering of the curve using the square elements depicted in figure 3.7, each δ^2 in area. The measured area, A_m, associated with the line is then

$$A_m = N\delta^2; \qquad (3.6a)$$

however, as δ tends to zero so does the measured area associated with the curve, i.e.

$$A_m \xrightarrow[\delta \to 0]{} 0. \qquad (3.6b)$$

This makes sense, as we expect a curve to have zero area. Similarly the measured volume, V_m, associated with the curve tends to zero as δ tends to zero, i.e.

$$V_m = N\delta^3 \qquad (3.7a)$$
$$N\delta^3 \xrightarrow[\delta \to 0]{} 0. \qquad (3.7b)$$

Extending the above to higher-dimensional measuring elements, we see that only the length measure of a smooth curve gives a finite, non-zero answer equal to the length of the curve, L.

If we require N hypercubes to cover an object then the measured hypervolume V_m^* is given by the number of hypercubes multiplied by the volume of each hypercube, i.e.

$$V_m^* = N\delta^{D_E}. \qquad (3.8a)$$

In the limit, as δ tends to zero, the measured hypervolume tends asymptotically to the actual hypervolume of the object, and is independent of δ, i.e.

$$V_m^* \xrightarrow[\delta \to 0]{} V^*. \qquad (3.8b)$$

However, as we saw from the measurement of the smooth curve above, the measurement
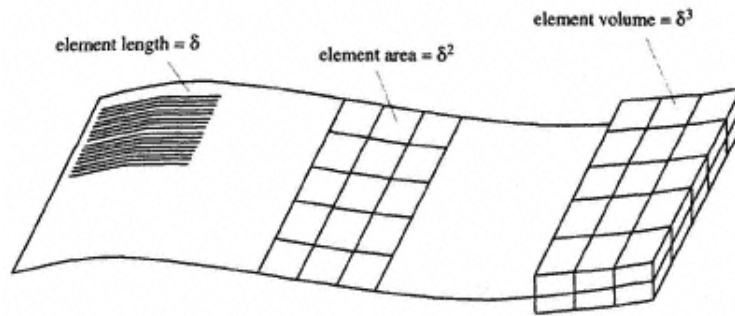

Figure 3.8.
Measuring a smooth surface.

obtained is only sensible as long as the dimension of the measuring elements and the object are the same. Alternatively, if we attempt to measure an object with an inappropriate measuring element then we find that the measured hypervolume either tends to infinity, for measuring elements (hypercubes) of dimension less than that of the object, or zero, if we use measuring elements of dimension greater than the object. As another example, consider trying to find the length, area or volume of a surface using line segments, squares or cubes, as shown in figure 3.8. We cannot cover a surface with a finite number of lines, thus the measured hypervolume, i.e. the measured 'length', of the surface diverges as the length of the measuring line segments, δ, tends to zero, i.e.

$$V_m^* = N\delta \qquad (3.9a)$$
$$N\delta \xrightarrow[\delta \to 0]{} \infty. \qquad (3.9b)$$

Here V_m^* is the one-dimensional hypervolume, i.e. length. Similarly if we attempt to cover a surface with cubes of volume δ^3 we find that the measured volume tends to zero as δ tends to zero, i.e.

$$V_m^* = N\delta^3 \qquad (3.10a)$$
$$N\delta^3 \xrightarrow[\delta \to 0]{} 0 \qquad (3.10b)$$

and in fact for all measuring hypercubes of dimension greater than three, the hypervolume tends to zero as δ tends to zero. Only when we measure the surface using 2D hypercubes, i.e. squares, do we find that the measured hypervolume tends to a finite value in the limit, i.e.

$$V_m^* = N\delta^2 \qquad (3.11a)$$
$$N\delta^2 \xrightarrow[\delta \to 0]{} V^* \qquad (3.11b)$$

where V^* is in fact the area of the surface, A.

We see from the above that the measured hypervolume depends critically on the dimension of the probing hypercubes used. Generally the measured hypervolume is either zero or infinity, the change from zero to infinity occurring when the appropriate dimension of the measuring hypercube is used. The Hausdorff dimension is based upon the above observation: in its definition we are allowed to consider hypercubes, or test functions, with hypervolumes δ^D where the exponent D is non-integer. The Hausdorff dimension D_H of the object is defined as the critical dimension, D, for which the measured hypervolume changes from zero to infinity.

The Hausdorff and box counting dimensions enable non-integer dimensions to be found for fractal curves. Take for example the Koch curve which has a topological dimension of one, a Euclidean dimension of two, and a similarity dimension of 1.2618. . . . We saw before that length is not a useful measure for the Koch curve since the measured length of the prefractal curve diverges as one iterates the generation process. If we tried to measure it with line elements one would find that its measured length would tend to infinity as we used smaller and smaller line segments. Its Hausdorff dimension is therefore greater than one. If instead we probed the Koch curve with square areas of side length δ we would find that its measured area tends to zero as δ tends to zero. Thus, the Hausdorff dimension is less than two. In fact, the Koch curve has a Hausdorff and box counting dimension equal to its similarity dimension of 1.2618 . . . .

In practice, it is not possible to probe objects with non-integer hypercubes, hence the Hausdorff dimension estimate is not useful for determining the fractal dimension of real objects. The box counting dimension is closely related to the Hausdorff dimension and in most cases both produce the same fractal dimension estimate. In addition, both the Hausdorff and box counting dimension will often produce the same dimension estimate as the similarity dimension. However, problems occur with self-crossing curves as the similarity dimension takes account of the multiple layering of the self-crossing curve (as we saw in chapter 2) whereas the Hausdorff and box counting dimensions do not.

3.5—
The Structured Walk Technique and the Divider Dimension

A commonly used method for determining a fractal dimension estimate of fractal curves in the plane is the structured walk technique, illustrated in figure 3.9. The technique is much faster to perform by hand than the box counting dimension and requires the use of a compass or a set of dividers. (A ruler may also be used if neither of the first two pieces of equipment is available, but this does result in a more laborious task.) The method is outlined as follows.
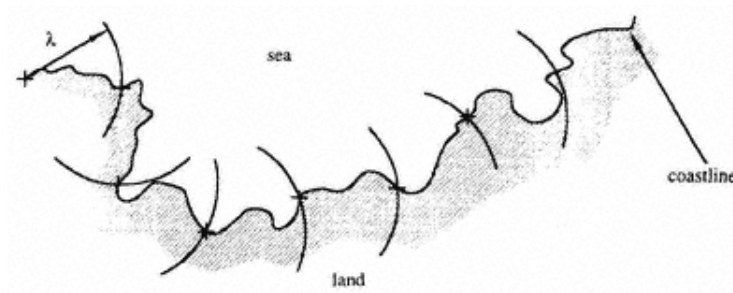
Figure 3.9.
Determining the fractal dimension of a coastline
using the structured walk technique.

(i) Set the compass/dividers at a step length λ.

(ii) Take the initial point at the beginning of the curve (or select a suitable starting position if it is a closed curve).

(iii) Draw an arc, centred at the initial point, which crosses the curve.

(iv) The point where the arc <u>first</u> crosses the curve becomes the centre of the next arc.

(v) Draw the next arc centred at the crossing point of step (iv).

  Repeat steps (iv) and (v) until the end of the curve is reached.

(vi) Plot $\log(L)$ versus $\log(\lambda)$, where L is the length of the coastline measured using λ as a step length, i.e. $L = N\lambda$, where N is the number of steps taken to 'walk' along the curve.
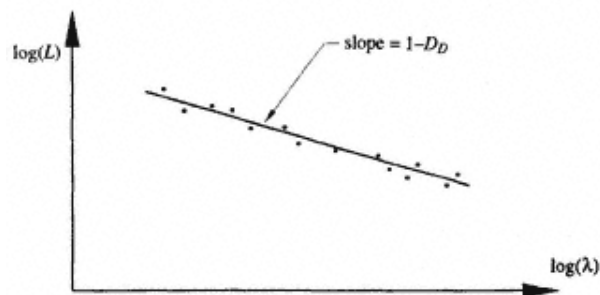

Figure 3.10.
Richardson plot obtained from
the structured walk technique.

(vii) Repeat steps (i) to (vi) for many step lengths, each time plotting $\log(L)$ versus $\log(\delta)$. The resulting plot is known as a **Richardson plot** (figure 3.10).

(viii) The slope, S, of the resulting curve is related to the **divider dimension, D_D,** by the relationship

$$S = 1 - D_D \qquad\qquad (3.12)$$

Hence, the dimension of the curve may be found by measuring S from the best fit line of the plotted points of step (vii). The slope of the Richardson plot is negative, i.e. the best fit line falls from left to right, thus $D_D > 1$. Note that when drawing successive arcs (steps (iv) and (v)) one may obtain slightly different dimension estimates depending upon the direction of approach of the arc. One may repeatedly swing clockwise into the coastline from the 'sea' (the inswing method), anti-clockwise out of the coastline from the 'land' (the outswing method), or alternate between the two (the alternate method). It is good practice to try all three methods and, in addition, to use various starting locations on the curve.
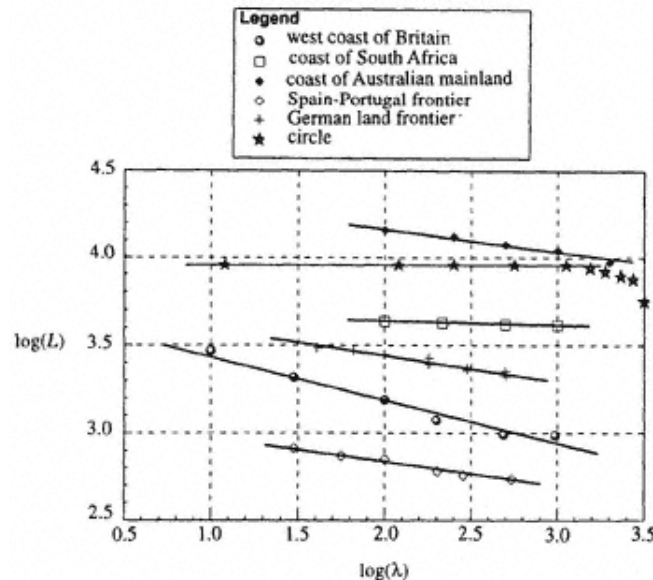

Figure 3.11.
Richardson plot of country boundaries.

Figure 3.11 contains a Richardson plot of original data by L F Richardson who noted that reported lengths of the border between two countries were often claimed to be different by the two countries involved. For example, he noted that the Spanish–Portuguese border was stated as being 987 km and 1214 km by Spain and Portugal respectively, and similarly the Dutch–Belgian border was stated as being 380 km and 449 km respectively by the two countries. After investigation he reasoned that the differences could be attributed to the length of the measuring stick used in the calculation of the boundary length. The smaller the measuring stick length, λ, the longer the measured length L was found to be. On the Richardson plot of figure 3.11 the data points for a circle are also plotted. Notice that the circle boundary slope tends to zero for small values of λ, as the divider dimension, D_D, tends to the topological dimension, D_T ($= 1$). This implies that the circle boundary is not a fractal, and more, in that it is a smooth curve with measurable length.
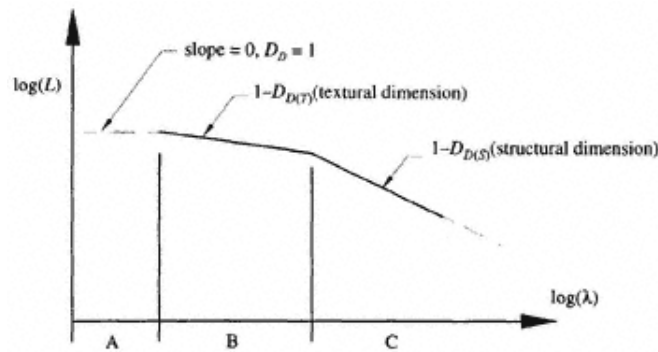
Figure 3.12.
Main regions of the Richardson plot.

Quite often there is more than one distinct slope to be found on a Richardson plot (typically three). Figure 3.12 shows the typical slopes that may be found on such a plot. From the figure, three distinct slopes may be seen: these correspond to three distinct regions of the object under investigation. These regions are summarized as follows.

(i) *Region A:* λ is very small. A natural fractal may not be self-similar below this scale or alternatively the resolution of the fractal may not be sufficient to allow investigation below these scales. Thus, the curve appears smooth at these levels of magnification and the dimension tends to unity.

(ii) *Region B:* Small λ. In this region we are measuring the fine scale structure, or texture, of the curve. This gives the **textural dimension**—'$D_{D(T)}$'.

(iii) *Region C:* Larger λ. Here we are now measuring the larger scale structure of the curve. This gives the **structural** *dimension*—'$D_{D(S)}$'.

Regions B and C correspond to two different fractals, intertwined with each other to form the curve. Objects with two or more fractal dimensions are known as **multifractals.**

One area where the divider dimension has been applied with particular success is as a characterization tool in the classification of the fractal boundaries of fine particles such as soots, powders and dusts. (See the notes at the end of this chapter.) Figure 3.13(*a*) contains a simulated soot particle made up of circles connected tangentially. The outer boundary of the particle reproduces the general features of profiles typically found in agglomerations of soot particles from exhaust emissions. Figure 3.13(*b*) contains the Richardson plot of the particle boundary in figure 3.13(*a*). Notice the two distinct slopes associated with the structure and texture of the particle.

The divider dimension is therefore an extremely useful tool. However, its main shortcoming is that it is limited to the investigation of curves in the plane. Should we wish to measure fractal objects other than curves, say for example the surface of a cloud or fractal landscape, the box counting dimension should be used; this, due to its versatility, may be used to probe all manner of fractal objects occurring in multi-dimensional spaces.
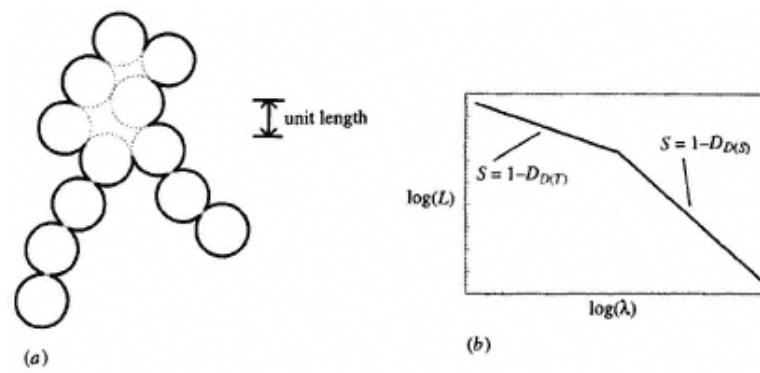
Figure 3.13.
Richardson plot of a synthetic particle boundary.
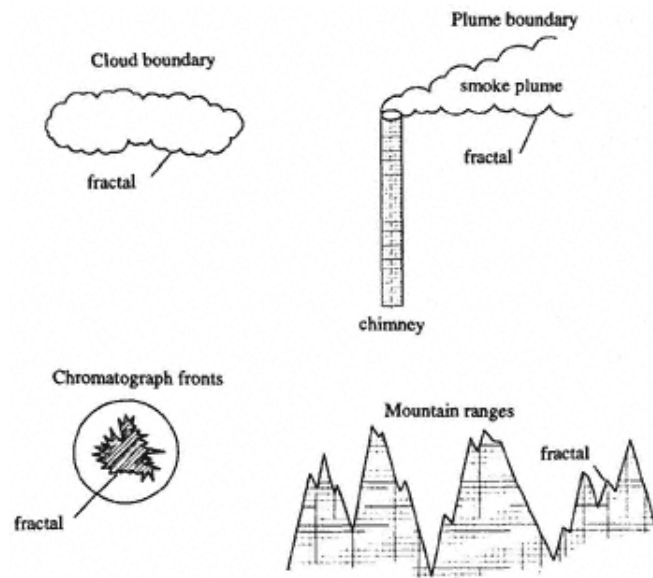(*a*) Synthetic particle. (*b*) Richardson plot.

Figure 3.14.
A selection of natural fractal objects.

Both the divider and box counting dimensions have been used to measure the fractal dimension of many natural fractals, including of course real coastlines and fineparticle boundaries, other examples include (see figure 3.14) cloud boundaries, smoke plume boundaries, chromatograph diffusion fronts, landscape profiles, and so on. Both dimension estimates are also useful in the estimation of the fractal dimension of crossing curves, such as fBm, which we shall encounter in chapter 4.

We leave this section by looking at the relationship between the box counting dimension and divider dimension on a fractal curve. First, we consider the box counting dimension. Rearranging equation (3.2) for non-unit hypervolumes we obtain

$$N(\delta)\delta^D = V^* \tag{3.13a}$$

where D is the box counting dimension. As an aid to clarity in the following discussion, we omit the subscript B of the box counting dimension and include δ in parenthesis to denote that N is a function of the box size δ. Hence, the number of boxes counted scales with δ as follows:

$$N(\delta) \propto \frac{1}{\delta^D} \tag{3.13b}$$

Considering now the structured walk technique, the measured length of the coastline, L, is a function of the divider length, λ, used, i.e.

$$N(\lambda)\lambda = L(\lambda). \tag{3.14}$$

Again, parentheses are used to denote that here the number of steps N required to walk along the curve, and hence the measured length L, is a function of step length λ. The linear scales in both techniques, δ and λ, are proportional to each other, i.e.

$$\lambda \propto \delta \tag{3.15a}$$

hence

$$N(\lambda) \propto N(\delta) \tag{3.15b}$$

Combining the above we obtain

$$\frac{1}{\lambda^D}\lambda \propto L(\lambda) \tag{3.16a}$$

or, more simply,

$$\lambda^{1-D} \propto L(\lambda). \tag{3.16b}$$

Hence, a log–log plot of λ against L results in a line with slope S equal to $1–D$. Here we can see that the box counting dimension is in fact equivalent to the divider dimension for coastline curves. It is important to note, however, that this relationship between D_D and D_B does not hold for a special class of fractals with anisotropic scaling. We will come across these fractals, known as self-affine fractals, in the following chapter.
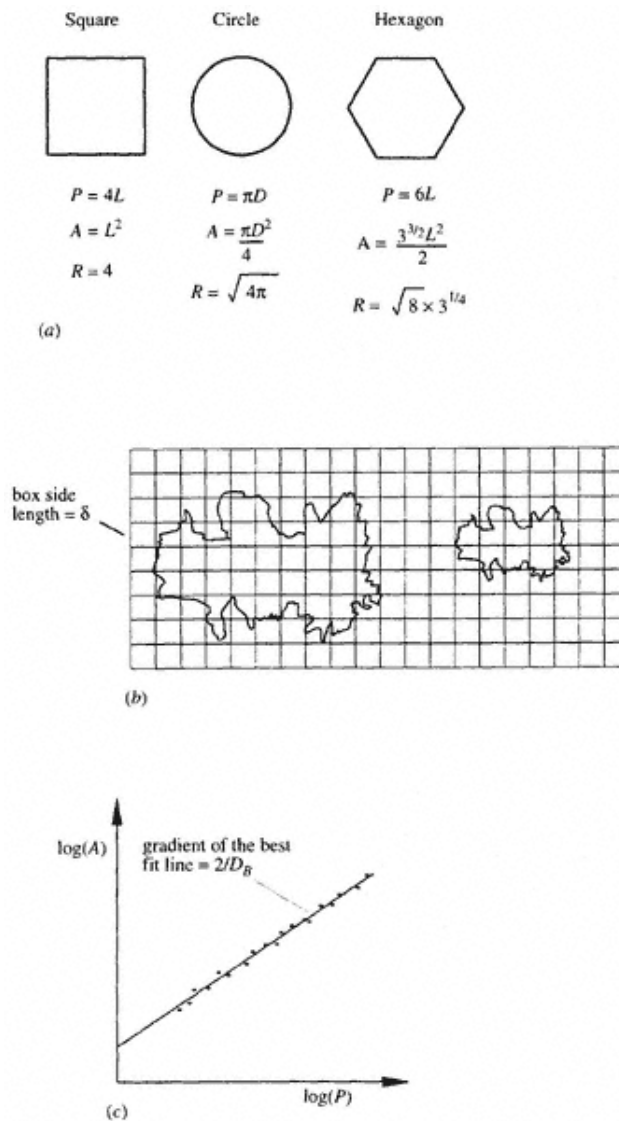
Square Circle Hexagon

$P = 4L$

$A = L^2$

$R = 4$

$P = \pi D$

$A = \dfrac{\pi D^2}{4}$

$R = \sqrt{4\pi}$

$P = 6L$

$A = \dfrac{3^{3/2} L^2}{2}$

$R = \sqrt{8 \times 3^{1/4}}$

(a)

box side
length = δ

(b)

$\log(A)$

gradient of the best
fit line = $2/D_B$

$\log(P)$

(c)

Figure 3.15.
The perimeter–area relationship for similarly shaped bounded
fractal islands. (a) Perimeter-area ratios, R, for common
Euclidean shapes: L is the side length, D is the diameter (R is
constant regardless of size of shape). (b) Similar islands
with fractal boundaries (note that δ must be small enough
to accurately measure the area of the smallest island).
(c) A logarithmic plot of A against P revealing fractal
dimension and self-similarity.

3.6—
The Perimeter-Area Relationship

We leave this chapter by briefly looking at an important relationship between an enclosed area, A, and its boundary perimeter, P, known as the **perimeter–area relationship.** For regular Euclidean shapes, i.e. circles, squares, triangles, hexagons, and so on, the ratio of the perimeter to the square root of enclosed area, R, is a constant regardless of the size of the shape, i.e.

$$R = \frac{P}{\sqrt{A}}. \qquad (3.17a)$$

for a square, circle and hexagon, R is 4, $\sqrt{4\pi}$ and $\sqrt{8} \times 3^{1/4}$ respectively (see figure 3.15(a)). We can generalize this rule for areas bounded by fractal curves, where the length of the perimeter diverges as we use smaller and smaller measuring sticks to measure it. To do this we modify equation (3.17a) to

$$R = \frac{P^{1/D_B}}{\sqrt{A}} \qquad (3.17b)$$

where P and A are now the measured perimeter and area of the boundary, using a length scale δ.

Equation (3.17b) is useful if, for example, we have a set of fractal shapes and we want to know whether they are statistically similar. Figure 3.15(b) shows a sketch of two random fractals islands at different scales. If these random fractals are the same shape then R given by equation (3.17b) should hold. In practice, we can investigate a whole series of fractal island shapes by covering them with a grid of box size δ. Then $P = N_p \delta$ and $A = N_a \delta$ where N_p and N_a are the numbers of boxes required to cover the perimeter and bounded area respectively. As long as we choose δ small enough to accurately measure the area of the smallest fractal island then a logarithmic plot of A against P for each island should produce a slope equal to $2/D_B$. This is illustrated in figure 3.15(c). In this way we can not only find the fractal dimension of the boundaries of a group of fractal islands, but also check that they are of similar shape. This technique has been used successfully to classify many sets of fractal shapes including rain clouds, fracture surfaces, contours and lake perimeters.

3.7—
Chapter Summary and Further Reading

3.7.1—
Chapter Keywords and Key Phrases

random fractals	*statistical self-similarity*	*Hausdorff dimension*
box counting method	*box counting dimension*	*structured walk technique*
Richardson plot	*divider dimension*	*structural dimension*
textural dimension	*multifractals*	*perimeter–area relationship*

3.7.2—
General.

In this chapter we investigated fractal objects which are not exactly self-similar in structure (as were those encountered in chapter 2), but rather statistically self-similar, with each small part of the fractal replicating the statistical properties of the whole. To determine the fractal dimension of these random fractals we may use the box counting dimension or the divider dimension (curves only). The similarity dimension used in chapter 2 cannot be used for random fractals as it relies on exact self-similarity. As with chapter 2, the reader is referred in the first instance to the excellent book, *The Fractal Geometry of Nature*, by Benoit Mandelbrot (1982a), for more information on the fractal geometry of random fractals. In addition, the text contains a wide ranging historical review. The book by Briggs (1992) contains many beautiful photographs of natural fractal phenomena. Another book by Hirst and Mandelbrot (1994) contains a series of striking black and white photographs used to illustrate the fractal geometry of landscapes. Mainieri (1993) gives criteria for the equality of the Hausdorff and box counting dimensions. More advanced mathematical accounts of fractal geometry are to be found in the texts by Falconer (1985, 1990), Edgar (1990), Wicks (1991), Dobrushin and Kosuka (1993), Massopust (1994), and Mattila (1995). Fractal curves are comprehensively dealt with by Tricot (1995).

The motivation behind much of the interest in fractal geometry lies in its ability to characterize natural phenomena (Kadanoff, 1986). It is now realized that there are a large number of objects and processes found in nature which may be described in terms of their fractal properties. In general, these phenomena exhibit statistical self-similarity over a large but finite range of scales. In the remainder of this section, many examples are given of naturally occurring objects and processes which have been described in terms of their fractal properties, together with references to allow the reader to delve more deeply into his or her own particular field of interest. In most cases, only essential references are given for the reader to use as a starting point for a more specific search. Note that there is some repetition of topics as many texts contain a wide range of fractal examples.

3.7.3—
Miscellaneous Subject Areas

Harrison (1995) provides an elementary introduction to **fractals in chemistry.** A general background on **fractal curves** and **fractal geometry,** as well as applications in chemistry, is given by Fan *et al* (1991): this monograph contains three detailed examples of the use of fractal concepts in real **chemical studies.** A comprehensive account of the uses of fractal geometry in heterogeneous chemistry is given in a collection of papers edited by Avnir (1989): the text illustrates many uses of fractal geometry to describe chemical substances and processes including the following: **polymers, aggregations, interfaces, electrodes, molecular diffusion, molecule surface interactions, reaction kinetics, adsorption, flow in porous media, chromatography, geochemistry** and **analysis of proteins.** Three papers by Coppens and Froment (1994, 1995a, b) detail diffusion and reaction in a **fractal catalyst.** An excellent collection of papers concerning **fractals in physics** is edited by Aharony and Feder (1990), and many of the papers are referenced individually within this text. Pietronero and Tossatti (1986) have also edited a collection

of papers concerning the use of **fractal geometry in physics.** This text covers a wide variety of topics including **viscous fingering, cracked metals, diffusion fronts** and the **fractal structure of clouds.** A comprehensive treatise on **fractal geometry and surface growth** is given by Barabási and Stanley (1995) (see DLA fractals in chapter 4). Fractals in **biology and medicine** are treated in a series of articles edited by Nonnenmacher *et al* (1994). The role of fractal geometry in **physiology** is outlined by West (1990) in the first half of his book (see also West and Goldberger 1987). The potential applications of fractals in **electrical engineering** are given by Jacquin (1994), and in a special section concerning the topic in the proceedings of the IEEE (1993). This latter publication contains the following topics: **wavelets and fractals, a review of fractal image coding, fractals in circuit output, computer interconnection, electrical processes in fractal geometry, radar imagery** and **the ultrasonic characterization of fractal media.**

Kaye (1994) uses fractal geometry to describe many of the properties of fractals in engineering, including: **fine particle boundaries, filter geometry, fractures, powder mixing, concrete, smoke plume boundaries** and **percolation.** This extensive text contains many real and synthetic particles (and other forms) together with their Richardson plots. (The **original Richardson plot** is to be found in the article by Richardson (1961).) In addition, the text includes an interesting chapter containing thoughts on the use of fractal geometry in the natural sciences. A review of the measurement of boundary fractal dimensions of highly irregular objects is given by Allen *et al* (1995). The reader interested in the use of fractal geometry in geology and geophysics is referred to the book by Turcotte (1992), who covers many diverse areas including **geological fragmentation,** the **fractal statistics of earthquakes,** the **fractal grading of ore deposits** and the **fractal structure of topographic images.** The structure of **soil fabric** has been described in terms of fractals by Bartoli *et al* (1991) and Young and Crawford (1991), and modelled using fractals by Moore and Krepfl (1991). Architects should see the book by Bovill (1996) for an introduction to fractal geometry in **architecture and design.**

Two excellent texts edited by Bunde and Havlin give many examples of the use of fractal geometry in science. The texts include coverage of the following topics: **cracks and fractures, dielectric breakdown, viscous fingering, smoke particle aggregates, chromatograph fronts, diffusion fronts** (Bunde and Havlin 1991); **neurons, lung (respiratory tree), polymer structure, DNA, chemical reactions, flow through porous media** (Bunde and Havlin 1994). The text edited by Cherbit (1991) treats the following topics: **galactic clusters, manganese oxide, electrochemistry, renal filtration, culture growth, lung structure, diffusion fronts** and **fractal dimension relative to observer.** A brief discussion of the fractal properties of **lightning, fluid turbulence** and **crystal growth** is given in the book by Schroeder (1991). Another text, edited by Fleischmann *et al* (1989), deals with fractals in the natural sciences and contains papers on, amongst other things, **fractals and phase transitions, structure of fractal solids, fractal aggregates, electrodeposition, flow through porous media** and **fractal adsorption.**

Other areas which have been investigated for their fractal properties are (in no particular order) the following: **the trajectories of drifters on the ocean surface,** (Osborne *et al* 1989) (see also chapter 4); **stock market indicators** (Huang and Yang 1995); **moon crater distribution** (Peitgen and Saupe 1988); the **structure of dispersing plumes** (Sykes and Gabruk 1994); **hydraulic roughness variations** (Vieux and Farajalla

1994); **fluid turbulence** (Sreenivasan 1991); **vegetative ecosystems** (Hastings and Sugihara 1993); **rain** (Lovejoy and Mandelbrot 1985); **cracks** (Ali *et al* 1992, Xie 1995) and **fractal crack models** (Bouchaud *et al* 1993); **the structure of the universe** (Peebles 1989, Gurzadyan and Kocharyan 1991, Coleman and Pietronero 1992); **fractal surfaces** (Min *et al* 1995); **the ocean floor** (Herzfeld *et al* 1995); **the structure of cities** (Batty and Longley 1986, Batty 1995); **sunspots** (Milovanov and Zelenyi 1993); **cement structures and diffusion therein** (Niklasson 1993); the optical properties of **fractal quantum wells** (Gourley *et al* 1993); **growth forms of sponges** (Kaandorp 1991); **music** (Hsü and Hsü 1992); **oil and gas reserves** (Poon *et al* 1993); **medicine** (Keipes *et al* 1993); **biology and medicine** (Havlin *et al* 1995); **human retinal vessels** (Family *et al* 1989); the **classification of Chinese landscape drawings** (Voss 1992); **evolution** (Vandewalle and Ausloos 1995); **the shape of broccoli and cauliflower** (Grey and Kjems 1989); **microscopy** (Cross 1994); **food research** (Peleg 1993); **stereological measurements** (Flook 1982); **superconductors** (Wang *et al* 1994); **fungal morphology** (Crawford *et al* 1993); **ocean waves** (Zosimov and Naugol'nykh 1994); **turbulent fluid jets** (Flohr and Olivari 1994); **communications networks and the fractal structure of population distributions** (Appleby 1995); **turbulent flames** (Smallwood *et al* 1995); **graphite shapes in cast irons** (Lu and Hellawell 1994); **pressure transient analysis in naturally fractured reservoirs** (Acuna *et al* 1995, Acuna and Yortsos 1995); **fractal electrodes** (Bolz *et al* 1995); **quasi-brittle fracture** (Bazant 1995).

3.7.4—
Perimeter-area Relationship

The perimeter–area relationship has been used extensively to characterize many sets of fractal objects in a whole range of scientific and engineering problems. References which specifically cite the use of the perimeter-area relationship include those by Mandelbrot *et al* (1984) and Mu and Lung (1988), who characterize the contours of **fracture surfaces of steel**; Pande *et al* (1987), who characterize **fractured titanium alloy;** Issa and Hammad (1994), who similarly use the technique to characterize **concrete fractures;** Nikora *et al* (1993) and Wu and Lai (1994), who investigate **river channels and drainage areas;** Krummel *et al* (1987), who characterize **deciduous forest patterns;** Goodchild (1988), who investigates the similarity of **lake forms** on a simulated landscape; Lovejoy (1982), Hentschel and Procaccia (1984) and Rys and Waldvogel (1986), who characterize **rain clouds and hail clouds.** The derivation of the perimeter–area relationship is explained simply in Hastings and Sugihara (1993). Cheng (1995) gives an up to date overview of generalized perimeter–area relationships. This paper also contains a brief application of the technique to **geochemical problems.**

3.7.5—
Erroneous Dimension Estimates

Finally, it should be mentioned that, under certain conditions, erroneous dimension estimates may be found for non-fractal data sets (Hamburger *et al* 1996) and great care should be taken when determining dimension estimates from real data.

3.8—
Revision Questions and Further Tasks

Q3.1 List the keywords and key phrases of this chapter and briefly jot down your understanding of them.

Q3.2 Use 3D hypercubes of side length δ to show that the box counting dimension of a plane lamina is two. It may help to draw a sketch using a square lamina with a side length of eight units, i.e. area = 64 units, and use values of δ which are powers of two, i.e. 2, 4, 8, etc. Plot $\log(N)$ against $\log(\delta)$ to obtain D_B.

Q3.3 (*a*) On graph paper show the construction of the triadic Cantor set to step $k = 4$. (Remember step $k = 0$ is the unit line.) Use 2D hypercubes of various side length δ to produce an estimate of the box counting dimension of the set. To do this plot *log(N)* against $\log(1/\delta)$ for various values of δ. Use values of δ which are integer powers of one third.

(*b*) Repeat (*a*) using a randomized triadic Cantor set generated by randomly selecting one third of the remaining line segments for removal at each stage in the construction (see the top of figure 3.1). How does the estimate compare with that obtained in (*a*)?

(*c*) What happens when you use δs which are not integer powers of one third in (*a*) and (*b*) above?

Q3.4 Use the structured walk technique to show that the divider dimension of a regular triadic Koch curve is equal to the similarity dimension of 1.26. . . . Use the large Koch curve provided in figure Q3.4, normalizing all step lengths by the base length. First use step lengths which are integer powers of one third of the base length, then investigate for yourself the effect of using step lengths which are not integer powers of one third of the base length.

Q3.5 From the Richardson plot of figure 3.11 in the text, determine the dimension of both the Spanish–Portuguese border and the west coast of Britain. In addition, determine the divider dimension of a circle at small scales. Explain the answers you obtain.

Q3.6 Count the number of boxes (N) that intersect the coastline of Iceland in figure Q3.6. Do this for both the large and small boxes. From the results estimate the fractal dimension of the coastline.

Q3.7 Explain, with the aid of a diagram, what is meant by the structure and texture of a fractal curve.

Q3.8 Use the structured walk technique to estimate the **structural** and **textural** divider dimensions of the rugged boundary given in figure Q3.8. Use the inswing, outswing and alternate methods beginning at points A–C in turn (i.e. nine walks in total).

Q3.9 Use the structured walk technique to estimate the **structural** and **textural** divider dimensions of the two synthetic soot particles in figure Q3.9. Again, for each particle, use the inswing, outswing and alternate methods beginning at points A–C in turn.

Q3.10 Calculate the fractal dimension of the coastline of mainland Scotland (figure Q3.10) from Mallaig to Portpatrick.

Q3.11 Select other coastlines from an atlas and find both the box counting dimension and the divider dimension. See how the two estimates compare.
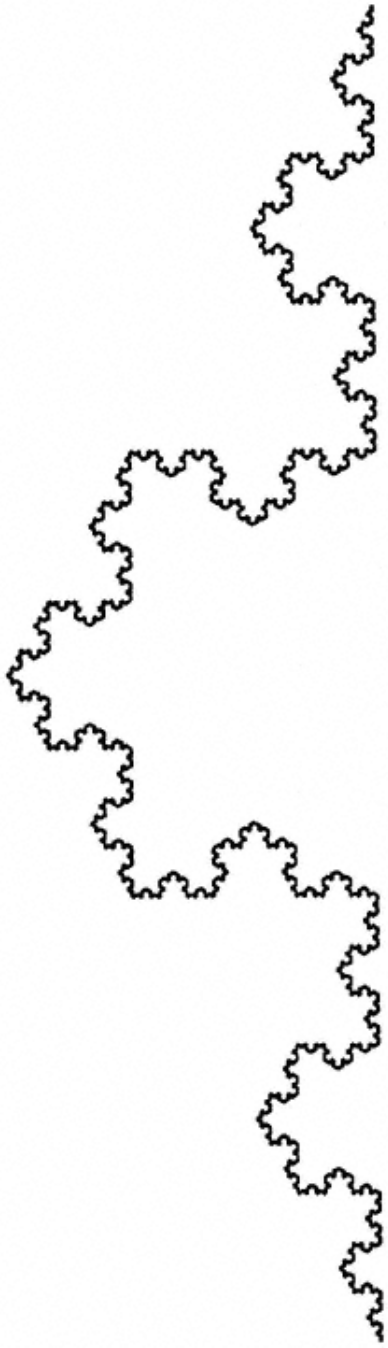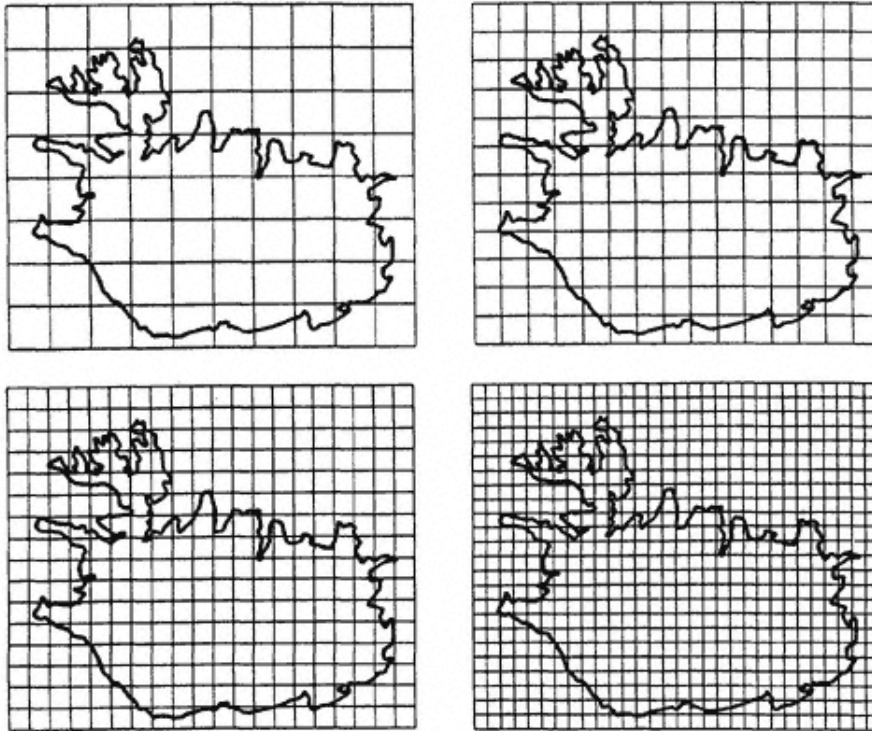
Figure Q3.4.
The Koch curve.

Figure Q3.6.
The coastline of Iceland.

Q3.12 (*a*) Plot log(P) against log(A) for three squares of different side length. Using the perimeter–area relationship, find the dimension of the perimeter from the plot.

(*b*) Repeat (*a*) for equilateral triangles.

(*c*) Consider Koch islands (figure 2.14) with arbitrary initiator lengths. Verify that the perimeter-area relationship will produce a dimension $D_B = 1.2618\ldots$ for the coastline of such a group of Koch islands.

(*d*) Try to find a group of random fractal island shapes and see whether they are of the same shape (in a statistical sense) using the perimeter-area relationship.

Q3.13 Think of natural curves, other than those mentioned in the text, which you believe may have fractal properties. Try to list at least five.
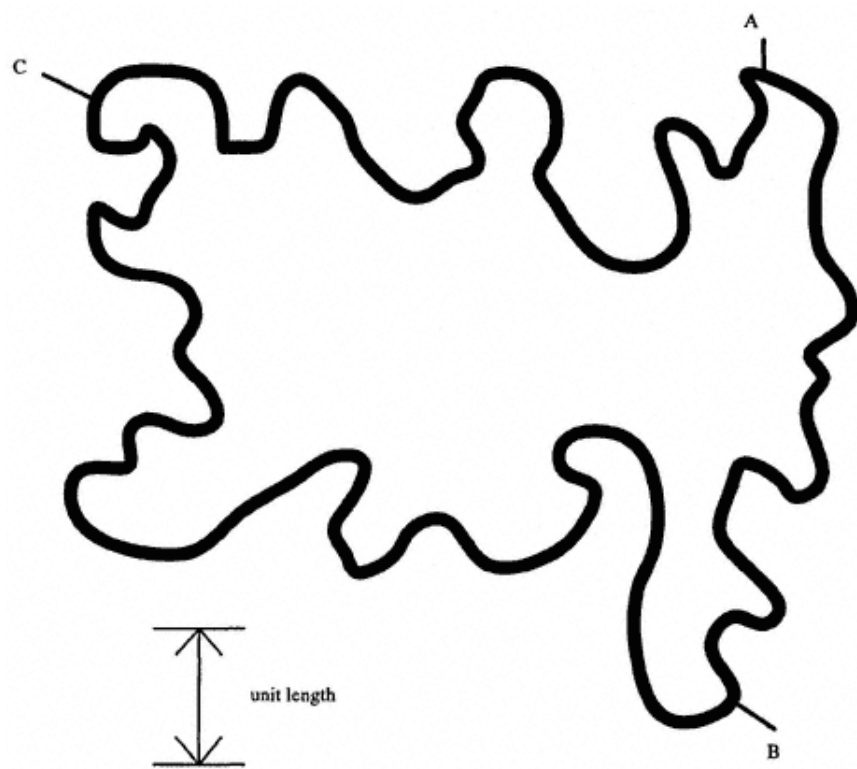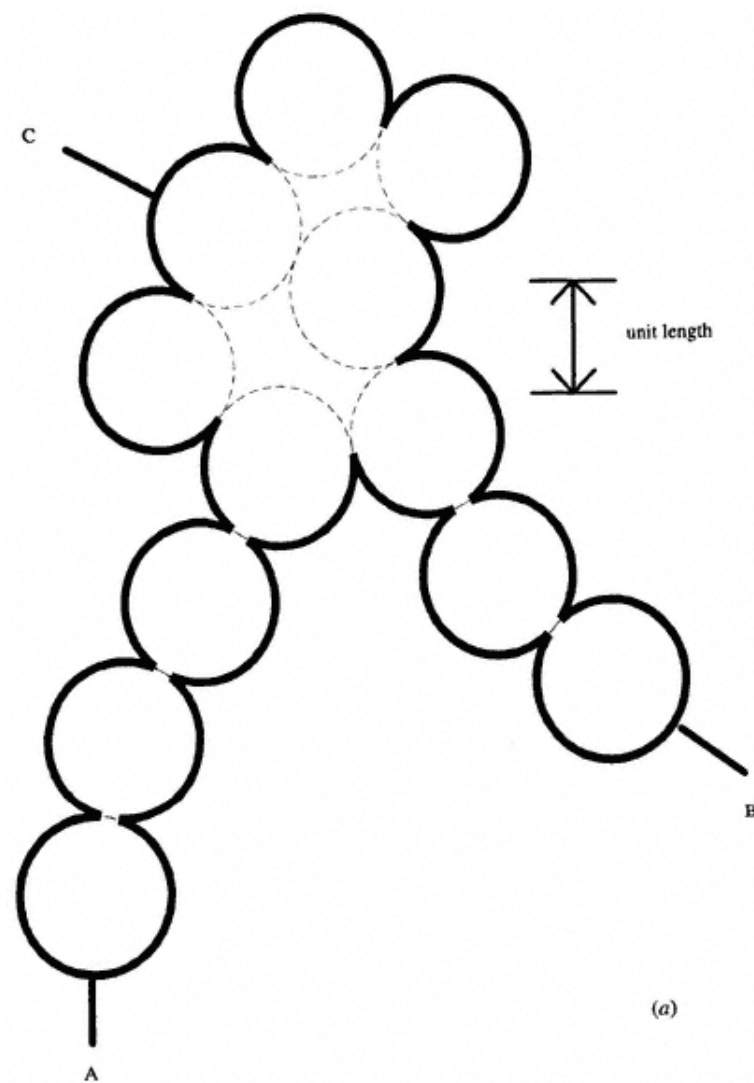
Figure Q3.8.
A rugged boundary.

Figure Q3.9.
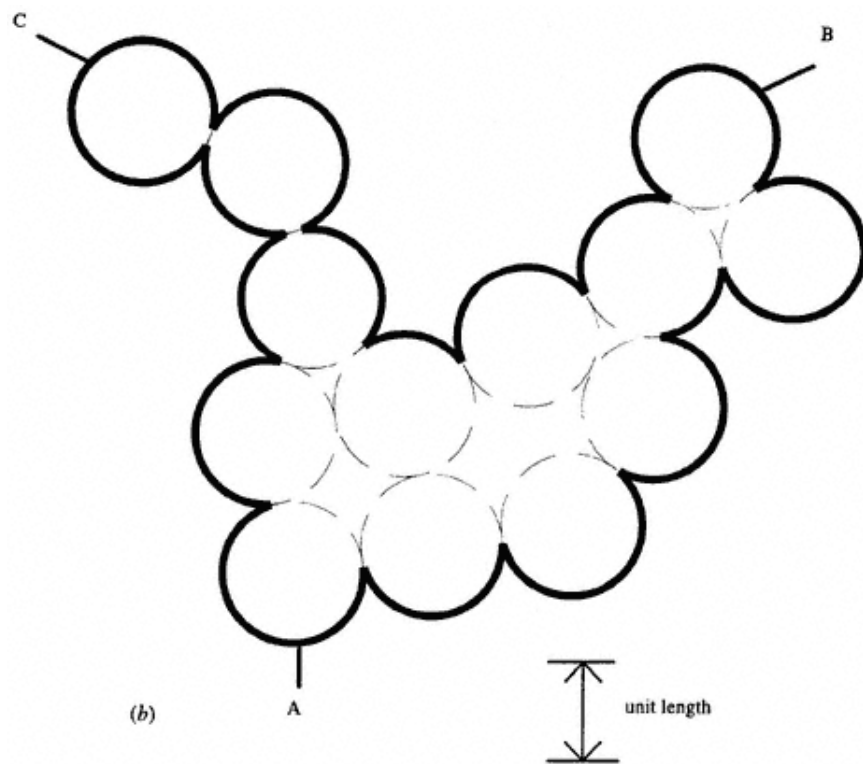(*a*) Synthetic soot particle 1. (*b*) Synthetic soot particle 2.

Figure Q3.9.
(*b*) Continued.

Figure Q3.10.
The western coastline of Scotland.